# Equation of state for 1,2-dichloroethane based on a hybrid data set

A fundamental equation of state in terms of the Helmholtz energy is presented for 1,2-dichloroethane. Due to a narrow experimental database, not only laboratory measurements but also molecular simulation data are applied to the fitting procedure. The present equation of state is valid from the triple point up to 560 K for pressures of up to 100 MPa. The accuracy of the equation is assessed in detail. Furthermore, a reasonable extrapolation behaviour is verified.

Keywords: 1,2-dichloroethane, equation of state, Helmholtz energy, hybrid data set, thermodynamic properties

## 1 Introduction

In modern process engineering, chemical industry, and academy research, there is an increasing demand for accurate thermodynamic properties. Nowadays, such information is provided by equations of state. Due to their fundamental nature, most accurate equations of state are given in terms of the Helmholtz energy with temperature and density as independent variables. Only less than ten substances are modelled in reference quality and an additional 120 substances are described by less accurate industrial equations of state. The thermodynamic properties of all other substances have to be calculated by means of, e.g., cubic equations of state such as those by Peng and Robinson [1] or Redlich and Kwong [2], physically based equations of state according to Statistical Associating Fluid Theory (SAFT) [3], the BACKONE equation of state [4, 5], or others like the Lee-Kesler equation of state [6]. The accuracy of correlation equations is highly dependent on the availability of experimental data, which are used for their fitting. Unfortunately, for many industrial fluids, there are insufficient experimental data available because experiments are time-consuming and expensive. Furthermore, many fluids exhibit challenging properties, such as toxicity, flammability, or corrosiveness, which render experiments in the laboratory particularly difficult.

Applying hybrid data sets (from experiments and molecular simulation) to the fitting procedure recently became a promising alternative. In the last years, significant progress was made in the field of molecular modelling and simulation so that the available experimental data sets can now be supplemented by molecular simulation data. An important advantage is that simulations are cheap and fast, and there are no restrictions with respect to challenging fluid properties. Furthermore, limitations of the experimental setup in terms of maximum temperatures or pressures do not apply. However, the accuracy of the simulation data are critically dependent on the quality of the underlying molecular model.

In this work, a fundamental equation of state for 1,2-dichloroethane (CAS No. 107-06-2) was developed. It is an oily and colourless fluid under standard conditions, slightly flammable, and toxic. When handling this substance, its narcotic, mutagenic, and carcinogenic properties have to be taken into account. It is used in numerous technical processes, e.g., it serves as an extracting agent for fats and oils as well as a solvent for resin and bitumen. The main application is the manufacturing of vinyl chloride, which is the basic product for polyvinyl chloride [7]. Up to date, there is no Helmholtz energy model for 1,2-dichloroethane available in the literature. Due to the limited database, the equation of state was fitted to experimental data from the literature [8–81] as well as molecular simulation data presented in this work.

## 2 Equation of state

The present equation of state is written in terms of the molar Helmholtz energy $a$, which is reduced by the universal gas constant $R = 8.3144621$ J·mol$^{-1}$ K$^{-1}$ according to Mohr and Taylor [82] and the temperature $T$

$$\alpha(\tau,\delta) = \frac{a(T,\rho)}{RT}. \tag{1}$$

For the calculation of specific properties, the molar mass $M = 98.9597$ g·mol$^{-1}$ [83] has to be applied. The Helmholtz energy is additively composed of an ideal gas (superscript o) and a residual (superscript r) contribution

$$\alpha(\tau,\delta) = \alpha^{\mathrm{o}}(\tau,\delta) + \alpha^{\mathrm{r}}(\tau,\delta), \tag{2}$$

where $\tau = T_\mathrm{c}/T$ and $\delta = \rho/\rho_\mathrm{c}$ with $T_\mathrm{c}$ and $\rho_\mathrm{c}$ being the critical values of temperature and density. The critical temperature $T_\mathrm{c} = 561.6$ K was taken from Garcia-Sanchez and Trejo [16]. The critical density $\rho_\mathrm{c} = 4.33$ mol·dm$^{-3}$ was determined during the fit so that the best representation of the experimental data was achieved, while a linear trend of the rectilinear diameter in the critical region and a distinct saddle point of the critical isotherm ($(\partial p/\partial\rho)_{T_\mathrm{c}} = 0$ and $(\partial^2 p/\partial\rho^2)_{T_\mathrm{c}} = 0$) was ensured.

The Helmholtz energy of the hypothetical ideal gas $\alpha^{\mathrm{o}}$ can be derived from an equation for the isobaric heat capacity of the ideal gas

$$\frac{c_p^{\mathrm{o}}}{R} = n_0 + \sum_{i=1}^{2} m_i \left(\frac{\theta_i}{T}\right)^2 \frac{\exp(\theta_i/T)}{\left(\exp(\theta_i/T)-1\right)^2}. \tag{3}$$

The constant $n_0$ refers to the temperature limit $T \rightarrow 0$ K, taking translation and rotation of the molecule into account. This simplified approach presumes that both effects are fully activated so that at least six degrees of freedom exist, leading to a zero temperature contribution $c_p^{\circ} = 4R$. The Planck-Einstein terms represent the vibrational modes, which have to be considered for every molecule consisting of more than one atom. Since vibration frequencies and the anharmonicities are not known with sufficient precision, a simplified approach according to Span [84] is applied. The parameters $m_i$ and $\theta_i$ are treated as adjustable parameters here. In this case, a 2-vibration model is sufficient to represent the available data within the required accuracy. For the determination of the parameters, ideal gas heat capacity data of Gwinn and Pitzer [72] were the only data set available for this fluid. Their experimental measurements were carried out with a flow calorimeter described by Pitzer and co-workers [85–87]. No information on sample purity or experimental uncertainty is given. Therefore, comparisons were made to isobaric heat capacity data of cyclohexane and cyclopentane in the ideal gas state, which were measured with the same apparatus. These data sets scatter within approximately 1 % around the equations of Zhou *et al*. [88] and Gedanitz *et al*. [89], respectively. Therefore, a similar uncertainty is expected for the data for 1,2-dichloroethane. In the paper by Gwinn and Pitzer [72] four different data sets are presented, which were determined by different modifications of the apparatus. Except for one data point at 335 K, all measurements agree with the present equation of state within the expected uncertainty (cf. Figure 1). Additional data of Gwinn and Pitzer [72], which were determined by theory, are reproduced within 1 % between 350 K and 1000 K (range of validity: $T > 200$ K). Outside of this region, deviations increase. During the fitting procedure, it turned out that the representation of these data cannot be improved without compromising the accuracy of other thermodynamic properties like

the speed of sound or the isobaric heat capacity. Since these measurements are expected to be more accurate than the $c_p^o$ data, the main focus was on a reasonable description of the speed of sound or the isobaric heat capacity and the deviations of the isobaric heat capacity of the ideal gas were accepted. Therefore, the uncertainty of the present equation of state is expected to be 1 % within the temperature range $T = 350$ K to 1000 K. The underlying parameters for Eq. (3) are $m_1 = 5.35$, $m_2 = 10.05$, $\theta_1 = 22.5$ K, and $\theta_2 = 2015$ K. For the application in the present Helmholtz energy model, a two-fold integration with respect to the temperature has to be carried out. The resulting reduced Helmholtz energy of the ideal gas is

$$\alpha^{\mathrm{o}}(\tau,\delta) = c^{\mathrm{II}} + c^{\mathrm{I}}\tau + 3\ln(\tau) + \sum_{i=1}^{2} m_i \ln\left(1-\exp\left(-\theta_i/T_{\mathrm{c}}\,\tau\right)\right) + \ln(\delta)\,. \tag{4}$$

The integration constants were determined such that $h_0 = 0$ J·kg$^{-1}$ and $s_0 = 0$ J·kg$^{-1}$·K$^{-1}$ at the normal boiling point temperature $T_{\mathrm{NBP}}(p_{\mathrm{v}} = 1$ atm) and saturated liquid density $\rho'(p_{\mathrm{v}} = 1$ atm): $c^{\mathrm{I}} = 0.972870308$ and $c^{\mathrm{II}} = 15.963798537$.

The residual contribution to the Helmholtz energy considers the intermolecular interactions in a real fluid. In contrast to the ideal gas, this contribution was described with an empirical expression that contains five polynomial, five exponential, and five Gaussian bell-shaped terms:

$$\begin{aligned}\alpha^{\mathrm{r}}(\tau,\delta) &= \alpha^{\mathrm{r}}_{\mathrm{Pol}}(\tau,\delta) + \alpha^{\mathrm{r}}_{\mathrm{Exp}}(\tau,\delta) + \alpha^{\mathrm{r}}_{\mathrm{GBS}}(\tau,\delta) \\ &= \sum_{i=1}^{5} n_i \delta^{d_i}\tau^{t_i} + \sum_{i=6}^{10} n_i \delta^{d_i}\tau^{t_i}\exp\left(-\delta^{p_i}\right) \\ &\quad + \sum_{i=11}^{15} n_i \delta^{d_i}\tau^{t_i}\exp\left(-\eta_i(\delta-\varepsilon_i)^2 - \beta_i(\tau-\gamma_i)^2\right).\end{aligned} \tag{5}$$

The corresponding parameters are listed in Table 1. For the determination of the required parameters, a non-linear algorithm provided by the National Institute of Standards and Technology was employed [90]. A brief description of the algorithm is

outlined in Lemmon and Jacobsen [91]. A non-published 14-terms equation for propane was used as initial solution for the fitting procedure. For a sufficiently accurate description of all available experimental data of 1,2-dichloroethane, one additional term was added here.

## 3 Comparison with experimental literature data

The accuracy of the present equation of state was established by comparison to the available experimental data from the literature. The statistical analysis was carried out by means of relative deviations according to

$$\Delta X = 100 \frac{X_{\mathrm{DATA}} - X_{\mathrm{EOS}}}{X_{\mathrm{DATA}}}, \tag{6}$$

and the average absolute relative deviation

$$AAD = \frac{1}{N} \sum_{i=1}^{N} \left| \Delta X_i \right|. \tag{7}$$

For homogeneous states, the *AAD* is discussed for gaseous and fluid state regions separately. Measurements in the supercritical state or in the critical region are not available. The thermal vapour-liquid equilibrium is divided into three temperature ranges: low temperature (LT: $T/T_c < 0.6$), medium temperature (MT: $0.6 \leq T/T_c \leq 0.98$), and high temperature (HT: $T/T_c > 0.98$).

### *3.1 Vapour-liquid equilibrium*

Comparisons of the vapour pressure data from the literature and calculated values from the present equation of state are presented in Table 2 and Figure 2. Additionally, correlations of the TDE [92] and DIPPR [93] data banks are included in the figure. The table shows that the vapour pressure was extensively investigated, but most of the data are located in a restricted temperature range of 270 K to 400 K. An

overview on all available vapour pressure data is illustrated in Figure 2 (top) and only the most recent and reliable data sets are depicted in Figure 2 (bottom). The data of Amireche-Ziar *et al*. [8] were measured with a static apparatus as described by Blondel-Telouk *et al*. [94]. The experimental uncertainties as specified by Amireche-Ziar *et al*. [8] yield a combined expanded uncertainty of (0.06 - 0.11) % and a sample purity of >99 % is stated. That agrees very well with the correlation of the data by the present equation of state up to 335 K (*AAD* = 0.080 %). The state points at $T = 344.8$ K and $T = 354.9$ K differ by more than 1 % from the present equation. Another accurate data set was published by Dohnal *et al*. [15], which is reproduced within 0.05 % (*AAD* = 0.021 %). A modified Dvořak-Boublík recirculation still (dynamic method) described by Boublíková and Lu [95] was used and the uncertainty analysis resulted in a temperature and pressure uncertainty of $\Delta T = 0.02$ K and $\Delta p = 7$ Pa, respectively. Deviations from the present equation of state and from other vapour pressure data from the literature show that the combined expanded uncertainty of 0.15 % to 0.2 % is probably too conservative. A third experimental data set was measured by Varushchenko *et al*. [37] with an ebulliometer in the same temperature range. The specified experimental uncertainties of $\Delta T = 0.004$ K and $\Delta p = 13$ Pa result in a combined expanded uncertainty of 0.03 % to 0.35 %. This is in good agreement with the present equation of state (*AAD* = 0.083 %). For $T < 250$ K, the data of Igoudjilene *et al*. [19] (*AAD* = 0.43 %) are underestimated by the present equation of state. During parametrisation, it was not possible to fit these data in a better way without compromising the representation of other properties. The correlation from the TDE [92] shows the same course as these data [19]. However, since other properties, such as density or speed of sound, were considered in addition to the vapour pressure, the course of the present equation of state is more meaningful than results from property-

specific vapour pressure equations. The high temperature range ($T > 400$ K) was investigated by Stull [33] and Garcia-Sanchez and Trejo [16]. The data of Stull [33] were not measured but collected from the literature and exhibit a huge deviation with respect to the present equation of state. Similar results were found for other fluids, e.g., for hexamethyldisiloxane [96] or ethylene oxide [97]. Therefore, these data were not considered in the development of the present equation of state. The measurements of Garcia-Sanchez and Trejo [16] were carried out with a sample purity of 99.7 % in a thick-walled Pyrex capillary tube. This technique was originally proposed by Ambrose [98] and used by McLure and Dickinson [99] to carry out vapour pressure measurements of hexamethyldisiloxane. As discussed in detail by Thol *et al*. [96], the experimental arrangement was questionable and the resulting vapour pressure data of hexamethyldisiloxane could only be reproduced within 2 %. For 1,2-dichloroethane, the representation is even worse. The investigated temperature range overlaps with other literature data from, e.g., Patel *et al*. [24] ($AAD = 0.55$ %) or Rollet *et al*. [29] ($AAD = 0.21$ %), which allows a closer investigation of the accuracy of these data. Figure 3 shows that the data of Patel *et al*. [24] and Rollet *et al*. [29] are in line with the accurate measurements of Amireche-Ziar *et al*. [8] and Dohnal *et al*. [15]. In the overlapping region, the data of Garcia-Sanchez and Trejo [16] systematically deviate by 4 % from other literature data and the present equation of state. Furthermore, a stepwise course of the data in the deviation plot is noticeable, cf. Figure 2 (bottom). This could be a consequence of the chosen calibration procedure: Nine chromel-to-alumel thermocouples, which were installed in the experimental setup, were calibrated to the critical temperatures of seven different alkanes reported by Ambrose [100]. Since these critical points significantly differ from each other, the stepwise course of the data is not surprising. Additionally, the uncertainty of the critical parameters increases with

increasing chain length of the alkanes. Finally, the specified uncertainties of 0.2 K and 10 kPa yield a combined expanded uncertainty of (0.5 - 13) %. Therefore, these data were not used to set up the present equation of state. Since these data were the only high temperature measurements, they were monitored during the fit so that they did not exceed a 4 % deviation. Therefore, the expected uncertainty of vapour pressure data calculated with the present equation of state is 0.1 % for $T < 400$ K and 4 % for higher temperatures.

The relative deviations of experimental saturated liquid density data from the present equation of state are illustrated in Figure 4. Measurements are only available between 293 K and 400 K. Since there are several different data sets of high accuracy available for homogeneous density data at atmospheric pressure, the saturated liquid density data were not applied to the fit. Nonetheless, all of the experimental data are represented within 0.5 %. Similar to the vapour pressure measurements, the data of Varushchenko *et al*. [50] (*AAD* = 0.036 %) are of very high accuracy and are reproduced within 0.06 %. Joshi *et al*. [44] (*AAD* = 0.015 %) determined their data by means of a pycnometer. Not much information is given on the purification grade or experimental uncertainties. However, their data are reproduced within 0.04 %. Considering possible irritations caused by sample impurities, this deviation is in good agreement with the specified overall experimental uncertainty of 0.0002 g·cm$^{-3}$ as stated by the authors. The experimental data for cyclohexane from the same publication as for 1,2-dichloroethane are reproduced with the equation of Zhou *et al*. [88] within 0.08 % (*AAD* = 0.04 %) although they were not considered during the development of the equation. Therefore, it can be assumed that the data are of high accuracy. Another data set was published by Klofutar *et al*. [45] (*AAD* = 0.066 %) and represented within 0.15 % by the present equation of state. No information is given on the measurement

device or experimental uncertainties. From the calibration fluids mentioned in Ref. [45] it can be concluded that an Anton Paar densimeter was used, which can yield very accurate results. Additionally, comparisons of their benzene measurements were made with the equation of Thol *et al*. [101]. For $T \leq 313$ K, these data agree with the equation within ±0.02 %. For higher temperatures, the deviations increase up to −0.32 %. The same trend is observed for 1,2-dichloroethane. For $T \leq 313$ K, the data are reproduced within ±0.06 %, whereas deviations increase up to −0.14 % for higher temperatures. An opposing trend was found for the saturated liquid density data of Kumagai and Takahashi [46] ($AAD = 0.20$ %). For increasing temperatures, the relative deviations from the present equation of state increase up to 0.45 %. Since these data are the only measurements between $T = 345$ K and 400 K, they cannot be confirmed.

The temperature range covered by experimental data is restricted so that it is difficult to assess the uncertainty of the present equation for this property. At least within $T = 285$ K and 400 K, deviations are 0.1 % to 0.45 %.

For the saturated vapour density, only one single state point is available and no statement on the accuracy of the present equation of state can be made. To ensure at least a correct qualitative behaviour, this line was adjusted by means of the rectilinear diameter $\rho_{\mathrm{RD}} = 0.5(\rho' + \rho'')$ [102].

If a fundamental equation of state is available, the vapour-liquid equilibrium can be calculated by means of the thermal, mechanical, and chemical equilibrium conditions. However, for computer calculations, it is helpful to use ancillary equations to generate initial values for density iterations. In this work, ancillary equations for vapour pressure, saturated liquid density, and saturated vapour density were developed:

$$\ln\left(\frac{p_{\mathrm{v}}}{p_{\mathrm{c}}}\right) = \left(\frac{T_{\mathrm{c}}}{T}\right)\sum_{i=1}^{5} n_i \left(1 - \frac{T}{T_{\mathrm{c}}}\right)^{t_i}, \tag{8}$$

$$\frac{\rho'}{\rho_c} = 1 + \sum_{i=1}^{4} n_i \left(1 - \frac{T}{T_c}\right)^{t_i}, \tag{9}$$

and

$$\ln\left(\frac{\rho''}{\rho_c}\right) = \sum_{i=1}^{6} n_i \left(1 - \frac{T}{T_c}\right)^{t_i}. \tag{10}$$

The corresponding parameters are given in Table 3.

### *3.2 Density of homogeneous states and thermal virial coefficients*

The representation of homogeneous density data with the present equation of state is summarized in Table 4 and illustrated in Figures 5 and 6. Only two data sets of Kumagai and Takahashi [46] and García-Giménez *et al*. [55] could be used to model the pressure dependence of the present equation of state. The measurements of Kumagai and Takahashi [46] are reproduced within 0.02 % to 0.37 % (*AAD* = 0.19 %). A systematic increase of the deviations with respect to the present equation of state can be observed for increasing temperatures and pressures. The data were measured with the same apparatus as the corresponding saturated liquid density data. The experiment was operated with a piezometer, which was sealed with mercury enclosed by two stainless-steel membranes. This movable part was connected to the core of a differential transformer. The sample was filled into a 4.5 cm³ borosilicate glass bulb, which was calibrated to less than 0.015 % in terms of the volume at atmospheric conditions. A mercury thermometer ($\Delta T$ = 0.05 K) was used to monitor the temperature of the thermostat and a Heise Bourdon gauge with an error of less than 0.1 MPa was used to pressurize the working oil and the sample. The volume change of the sample due to temperature and pressure variation was detected through the displacement of the core. The error in the determination of the displacement was stated to be 0.03 mm, but no mathematical formulation is provided to calculate the influence on the uncertainty of the density. Additionally, no information about the differential transformer is given. Thus, it

is not possible to explain the pressure-related increase of the deviations. However, a temperature gradient could be suspected in the apparatus. The upper part was subject to atmospheric conditions, whereas the lower part was heated. With increasing temperature, the temperature gradient rises and the influence is higher. Since there are no other experimental data available in this region, additional investigations are necessary to clarify if this behaviour is caused by the present equation of state or the measurements.

The low temperature and pressure region was explored by García-Giménez *et al*. [55] (*AAD* = 0.010 %). Data were measured with an Anton Paar vibrating-tube densimeter (DMA 512) with a high pressure cell. The temperature was stable within 0.01 K, whereas the pressure was adjusted with 0.005 % of the full scale. With these numbers and a specified uncertainty of $10^{-4}$ g·cm$^{-3}$ in terms of density, a combined expanded uncertainty of 0.019 % follows. Except for five state points, all of these data are reproduced within this uncertainty. Considering the sample purity of 99.7 %, these outliers (deviations of up to 0.03 %) are still reproduced within their experimental uncertainty. Therefore, it is assumed that the increasing deviation of the data of Kumagai and Takahashi [46] is due to the experimental data. Unfortunately, the measurements of the two author groups only overlap at a single state point. At $T$ = 298.15 K and $p$ = 10 MPa, the density of García-Giménez *et al*. [55] is reproduced within 0.0068 %, whereas the one of Kumagai and Takahashi [46] differs by 0.0307 % from the present equation. Hence, the data set of Kumagai and Takahashi [46] is assumed to be less accurate. Additional measurements of Kumagai and Takahashi [46] for ammonia carried out with the same apparatus are reproduced within 0.4 % with a preliminary equation of state by Lemmon [103]. Thus, the deviations for 1,2-dichloroethane are assumed to be reasonable.

In Figure 6, relative deviations of homogeneous density data measured at atmospheric pressure are presented. Similar to the saturated liquid density, the temperature range is restricted. However, there are several comprehensive data sets available, which are reproduced within 0.12 %. In Figure 6 (top), the impression of a wrong curvature of the equation could arise when considering the course of the measurements of Valtz *et al*. [64] (*AAD* = 0.010 %) and Manfredini *et al*. [60] (*AAD* = 0.043 %). Both data sets could not be fitted in a better way without compromising the homogeneous density data of García-Giménez *et al*. [55]. When deleting the data of Valtz *et al*. [64] and Manfredini *et al*. [60] from the plot, cf. Figure 6 (bottom), the eye-catching curvature is not apparent anymore and the remaining data scatter equally distributed around the present equation. Valtz *et al*. [64] carried out their measurements with a vibrating-tube densimeter (Anton Paar, DMA500) and a sample purity of 99.8 %. The densimeter was calibrated with dry air and water at $T = 293.15$ K, but no information is given how the temperature dependence was compensated. Manfredini *et al*. [60] also used a vibrating-tube densimeter (Anton Paar, DMA 60). The same purification grade as for the measurements of Valtz *et al*. [64] is reported. They claim the sample to be contaminated with 0.1 % water. When applying a simple linear combination of the mixture 1,2-dichloroethane (99.9 %) and water (0.01 %), the density of pure 1,2-dichloroethane would be reduced by 0.025 %. This is a possible explanation of the systematic shift with respect to the measurements of Valtz *et al*. [64]. However, the data of Valtz *et al*. [64] and Manfredini *et al*. [60] are still reproduced within 0.04 % and 0.11 %, respectively.

Based on the discussion above, the uncertainty of homogeneous density data calculated with the present equation of state is expected to be 0.05 % for $T < 320$ K and

$p < 20$ MPa, whereas for higher temperatures and pressures the uncertainty increases up to 0.5 %.

Three data sets for the second virial coefficient from the literature are shown as absolute deviations from the present equation of state in Figure 7. The data of Sewell and Stock [30] ($T = 273$ K to 323 K) were derived from the Berthelot equation fitted to experimental vapour pressure measurements ($AAD_{pv} = 0.80$ %) carried out by the same authors. The absolute deviations of 3.8 $cm^3 \cdot mol^{-1}$ with respect to the present equation of state (corresponding to a relative deviation of 0.4 %) without applying the data to the fit proves that this is a reasonable approach. Higher temperatures were investigated by Bohmhammel and Mannchen [79] and their data are reproduced within 40 $cm^3 \cdot mol^{-1}$ (5 %), but their information on experimental uncertainties is insufficient to assess the accuracy of these data. Finally, the data of Paniego *et al*. [81] differ by more than 250 $cm^3 \cdot mol^{-1}$ (20 %) from the present equation of state. Since the corresponding temperature range is covered by the reasonable data of Bohmhammel and Mannchen [79], the data of Paniego *et al*. [81] were not considered for the validation of the present equation of state.

### *3.3 Caloric properties*

In Figure 8, relative deviations of experimental speed of sound data from the present equation of state are depicted. All of them were measured at atmospheric pressure and differ from the present equation of state by less than 1 %. Although the publication from 1949 is rather old, data of Lagemann *et al*. [57] were applied to the fit. Their measurements were carried out with a variable-path ultrasonic interferometer as described by McMillan and Lagemann [104]. No information on the experimental uncertainty is given. Therefore, comparisons of their measurements on benzene and heavy water with the corresponding equations of state from the literature [101, 105]

were made. The calculated deviations do not exceed 0.5 %, without being applied to the fitting procedure of the corresponding equations. Thus, it is assumed to be reasonable to apply the data of Lagemann *et al*. [57] to model the temperature range from 270 K to 325 K. Good agreement with measurements by Bhatia *et al*. [52] (*AAD* = 0.074 %), Nath and co-workers [66–69] (*AAD* = 0.053 % to 0.019 %), and Sekhar *et al*. [70] (*AAD* = 0.092 %) supports this choice. In contrast, two quite recently published data sets of Ali and Tariq [40] and Oswal *et al*. [61] exhibit a different trend. Ali and Tariq [40] (*AAD* = 0.65 %) carried out their measurements with a single crystal variable path ultrasonic interferometer. The specified experimental uncertainty of 1 $m \cdot s^{-1}$ (corresponding to 0.09 %) was assessed by comparing their measurements to other literature data. However, their measurements on benzene, which were published in the same paper, differ by up to 4 $m \cdot s^{-1}$ (corresponding to 0.3 %) from the respective equation of state of Thol *et al*. [101]. Therefore, the uncertainty statement of Ali and Tariq [40] is questionable. Oswal *et al*. [61] (*AAD* = 0.41 %) state the same experimental uncertainty, but do not give any information how this value was determined. Thus, on the basis of all available data, except for the ones of Ali and Tariq [40], the expected uncertainty of speed of sound values calculated with the present equation of state is estimated to be 0.5 % at atmospheric pressure.

An overview about the available experimental isobaric heat capacity data is given in Figure 9. Only three data sets with more than two data points are available. Góralski *et al*. [71] (*AAD* = 0.097 %) measured their data by differential scanning calorimetry as described by Becker *et al*. [106]. The experimental setup as well as the measuring procedure is described very comprehensively and they claim a combined experimental uncertainty of 0.15 %, excluding the effect of sample impurity. Test measurements on water (maximum deviation 0.14 % with respect to the IAPWS-95 [107]) verify this

specification. Experimental data for toluene differ by up to 0.25 %, which is reasonable because the underlying equation of state [108] does not exhibit reference quality. Thus, the present equation of state for 1,2-dichloroethane was modelled so that the experimental uncertainty of 0.15 % was maintained. The data set of Rastorguev and Ganiev [74] (*AAD* = 0.69 %) was measured in the same temperature range. It differs by up to 1 % from the present equation and the data of Góralski *et al*. [71], and no information on the experimental uncertainties is available. The data set of Gwinn and Pitzer [72] (*AAD* = 0.26 %) is located in the gaseous phase and covers the temperature range between 379 K and 557 K. As mentioned in the discussion of the ideal gas heat capacity, no information on sample purity or experimental uncertainties is given. Measurements of the isobaric heat capacity for cyclohexane and cyclopentane [87] carried out with the same apparatus exhibit deviations of up to 1 % with respect to the equations of state of Zhou *et al*. [88] and Gedanitz *et al*. [89], which is at the same time the experimental uncertainty of the data. Based on these findings, the experimental uncertainty of the measurements for 1,2-dichloroethane is also expected to be 1 % and the representation with the present equation of state is supposed to be reasonable. The expected uncertainty of isobaric heat capacity data calculated with the present equation of state is thus claimed to be 1 % in the gaseous region and 0.2 % in the liquid state at $p$ = 1 atm.

For the heat of vaporization, only few measurements are available. Since this property is closely related to the vapour pressure, these data were only used for comparison. The data of Majer *et al*. [78], McGovern [22], and Rao and Viswanath [80] are reproduced within 0.4 % and, therefore, verify the behaviour of the vapour pressure curve.

## 4 Molecular simulation

Based on the available experimental data, the present equation of state for 1,2-dichloroethane is valid for temperatures from the triple point up to 560 K and pressures up to 100 MPa. Similar to the equations of hexamethyldisiloxane [96] and octamethylcyclotetrasiloxane [109], it was extended to a maximum temperature $T_{max} = 1000$ K and pressure $p_{max} = 1200$ MPa by means of molecular simulation data (cf. Figure 10, where $A_{mn}^{r}$ denote the molecular simulation data). The underlying molecular interaction model that was developed here consists of four Lennard-Jones (LJ) sites representing the two chlorine atoms and the two methylene groups ($CH_2$), and a point quadrupole in the centre of mass, cf. Figure 11. Therefore, the total intermolecular interaction energy in this case writes as

$$U = \sum_{i=1}^{N-1} \sum_{j=i+1}^{N} \left\{ \sum_{a=1}^{S_i^{LJ}} \sum_{b=1}^{S_j^{LJ}} 4\varepsilon_{iajb} \left[ \left( \frac{\sigma_{iajb}}{r_{iajb}} \right)^{12} - \left( \frac{\sigma_{iajb}}{r_{iajb}} \right)^{6} \right] + \frac{Q_i Q_j}{r_{ij}^5} \cdot f(\boldsymbol{\omega}_i, \boldsymbol{\omega}_j) \right\}, \qquad (11)$$

where $\varepsilon_{iajb}$ and $\sigma_{iajb}$ are the LJ energy and size parameters for the pair-wise interaction between LJ site a on molecule $i$ and LJ site b on molecule $j$. The distance between two sites or molecules is denoted by $r_{iajb}$ or $r_{ij}$, respectively. In case of the electrostatic interaction $Q$ stands for the quadrupole moment, which is dependent on the orientations $\boldsymbol{\omega}_i$ and $\boldsymbol{\omega}_j$ of molecules $i$ and $j$ according to [110, 111]. Finally, the summation limits $N$ and $S_x^{LJ}$ denote the number of molecules and the number of LJ sites, respectively.

The geometry of the molecule as well as the magnitude and orientation of its quadrupole were initially determined on the basis of quantum chemical calculations. Since 1,2-dichloroethane is a rather compact molecule, its internal degrees of freedom were neglected in the present simulations. However, it has to be noted that the assumption of rigidity is an oversimplification for this molecule, due to the significant

influence of other possible conformers on the thermophysical properties. These inherent model limitations are tackled by fitting vapour pressure and saturated liquid density data to experimental values by varying the LJ energy and size parameters of all LJ sites. The resulting parameters are listed in Table 5. Throughout, the simulations were carried out by using cut-off radii equal to half the simulation box sizes using 864 particles. LJ long-range interactions beyond the cut-off radius were corrected as proposed by Lustig [113]. The electrostatic long-range interactions were corrected with the reaction field method [110].

In order to calculate vapour-liquid equilibrium properties, the grand equilibrium method was used [115]. In this two-step procedure, the coexisting phases are simulated independently. In the first step, a Monte Carlo *NpT* ensemble simulation in the liquid phase is carried out to obtain the chemical potential as a function of pressure. This was done here with the gradual insertion method [117, 118]. After sufficient equilibration, the production is typically carried out for 500000 cycles. In the second step, a pseudo-grand canonical ($\mu VT$) ensemble simulation, which yields the saturated vapour state point, is carried out. Vapour pressure data are reproduced within 3.5 % for $T > 375$ K (cf. Figure 2). For lower temperatures, simulations were not feasible due to sampling problems. The saturated liquid density deviates from the present equation of state by 0.5 % for $T < 400$ K (cf. Figure 4). For higher temperatures, deviations increase. These values are well within the expected accuracy of a molecular model [112]. The representation of the homogeneous state properties by molecular simulation is presented in Figures 12 and 13. The simulated density data scatter around the present equation of state within 0.2 %. Keeping in mind that the experimental data are represented within 0.05 % for $T < 320$ K and $p < 20$ MPa (except for $p = 1$ atm) as well as 0.5 % for higher temperatures and pressures, the density data from molecular simulation are remarkably

good. The simulated speed of sound data exhibit a systematic deviation of approximately 3 %. For regions where no measurements are available, this uncertainty is acceptable.

After the verification of the molecular model, derivatives of the residual Helmholtz energy were simulated. Based on a methodology by Lustig [114], Thol *et al*. [116] comprehensively presented a new strategy for the development of Helmholtz energy equations of state based on molecular simulation data. In comparison to other literature, the innovation of this strategy is to simulate the residual Helmholtz energy and its derivatives with respect to the natural variables systematically:

$$A_{mn} = A_{mn}^{\mathrm{o}} + A_{mn}^{\mathrm{r}} = \tau^m \delta^n \frac{\partial^{m+n}\left(\alpha^{\mathrm{o}} + \alpha^{\mathrm{r}}\right)}{\partial\tau^m \partial\delta^n}. \tag{12}$$

Since the ideal gas contribution is given by the isobaric heat capacity of the ideal gas (cf. Eq. (3)), only the residual contribution to the Helmholtz energy is needed. In this work, the simulation data were generated by sampling 83 state points with the simulation tool *ms*2 [119]. At each state point, 864 particles were sufficiently equilibrated and then sampled for 2 million cycles with Monte Carlo *NVT* ensemble simulations. From one simulation run, all Helmholtz derivatives up to the third order (except for the third density derivative) were computed. Numerical simulation values along with their statistical uncertainties are given in the supplementary material. These simulation data allow the direct adjustment of the fundamental function and its derivatives with respect to the natural variables during the development of the equation of state. Comparisons of these data with the present equation of state are illustrated in Figure 14. Relative deviations of the residual Helmholtz energy $A_{00}^{\mathrm{r}}$ are 15 %. The first derivatives of the residual Helmholtz energy with respect to the density $A_{01}^{\mathrm{r}}$ and

temperature $A_{10}^{\mathrm{r}}$ as well as the first mixed derivative $A_{11}^{\mathrm{r}}$ are reproduced within 10 %. The second derivative of the residual Helmholtz energy with respect to the density $A_{02}^{\mathrm{r}}$ deviates up to 20 %, whereas the second derivative of the residual Helmholtz energy with respect to the temperature $A_{20}^{\mathrm{r}}$ differs by up to 40 %. This is most probably the reason for the systematic offset of the simulated speed of sound data depicted in Figure 13. For a better assessment of the quality of the data, the simulated Helmholtz derivatives are transferred to common thermodynamic properties according to the following relations [84]:

$$p/(\rho RT) = 1 + A_{01}^{\mathrm{r}}, \tag{13}$$

$$c_v/R = -\left(A_{20}^{\mathrm{o}} + A_{20}^{\mathrm{r}}\right), \tag{14}$$

$$c_p/R = -\left(A_{20}^{\mathrm{o}} + A_{20}^{\mathrm{r}}\right) + \frac{\left(1 + A_{01}^{\mathrm{r}} - A_{11}^{\mathrm{r}}\right)^2}{1 + 2A_{01}^{\mathrm{r}} + A_{02}^{\mathrm{r}}}, \tag{15}$$

and

$$w^2 M/(RT) = 1 + 2A_{01}^{\mathrm{r}} + A_{02}^{\mathrm{r}} - \frac{\left(1 + A_{01}^{\mathrm{r}} - A_{11}^{\mathrm{r}}\right)^2}{A_{20}^{\mathrm{o}} + A_{20}^{\mathrm{r}}}. \tag{16}$$

These results are compared to the present equation of state in Figure 15. The test simulations of the homogeneous density presented in Figure 12 already indicated a very good accuracy of the data. Here, the molecular simulation data are reproduced within 0.6 % for $\rho \geq 5$ mol·dm$^{-3}$. For lower densities, deviations increase up to 4 %. The physical behaviour of the present equation of state in this region was carefully monitored during the fitting procedure. Therefore, this effect is most probably caused by the simulation data. However, since no experimental measurements for 1,2-dichloroethane are available in the vapour state, a reliable statement cannot be made here. The simulated isochoric heat capacity scatters around the present equation within 2 % for $\rho \leq 2$ mol·dm$^{-3}$.

## 5 Physical and extrapolation behaviour

Selected diagrams to verify the physical and extrapolation behaviour of the present equation of state are illustrated in Figure 16. On the top (left), the vapour-liquid equilibrium including the rectilinear diameter is presented and no unreasonable behaviour was detected. The rectilinear diameter ends up as a straight line in the critical region und the critical isotherm exhibits a distinctive saddle point according to the pressure derivatives $\left(\partial p/\partial \rho\right)_{T\mathrm{c}} = 0$ and $\left(\partial^2 p/\partial \rho^2\right)_{T\mathrm{c}} = 0$. On the top (right), the speed of sound as a function of temperature along selected isobars proves correct physical behaviour. The saturated liquid phase exhibits a straight line with negative slope down to very low temperatures. Additionally, the saturated liquid and vapour lines merge in a minimum at the critical temperature. This is in accordance with a correct course of the isochoric and isobaric heat capacities, where the saturation lines merge in a distinct maximum. The correct behaviour of the phase identification parameter [120] (centre of Figure 16) was discussed in detail by Thol *et al*. [116] and Gao *et al*. [121]. Originally, this property was proposed to discriminate between liquid and vapour states without carrying out time-consuming flash iterations. In the context of developing equations of state, this property is valuable due to the high-order Helmholtz energy derivatives, which are involved. Therefore, wrong shapes of equations of state can easily be detected and revised. For the present equation, no inadequate changes in slope or curvature can be observed. On the bottom of Figure 16, the thermal virial coefficients up to the fourth order (left) and the characteristic ideal curves [122] (right) are presented. The second virial coefficient behaves as expected. The maximum of the third virial coefficient occurs slightly below the critical temperature. 1,2-dichloroethane is slightly associating and, therefore, a shift of the maximum is reasonable. However, this phenomenon is not proven experimentally yet, but only shown for simple potential models, such as the

Lennard-Jones fluid [116, 123]. The same applies for the fourth virial coefficient. It approaches negative infinity for $T \rightarrow 0$ K and a maximum is reached at the critical temperature. The absolute values are negative over the entire temperature range, which should actually remain positive beyond the maximum. However, this behaviour does not affect the calculation of thermodynamic properties for 1,2-dichloroethane within the specified uncertainties. Finally, no unreasonable changes in slope or curvature can be detected in the characteristic ideal curves [122]. Other typical diagrams, e.g., the $p\rho T$ relation at extreme conditions, the heat capacities, or the Grüneisen coefficient [124] were monitored as well and assessed to be reliable. Therefore, the physical as well as the extrapolation behaviour of the present equation of state is assumed to be correct.

## 6 Conclusion

The present equation of state for 1,2-dichloroethane is written in terms of the reduced Helmholtz energy, allowing for the calculation of any thermodynamic state property by a combination of its derivatives. The ideal contribution consists of two Planck-Einstein terms, whereas the residual contribution comprises five polynomial, five exponential, and five Gaussian bell-shaped terms. Based on the available experimental data set, it is valid for $T = 237.52$ K to 560 K and pressures of up to $p = 100$ MPa. The expected uncertainty of vapour pressure data calculated with the present equation of state is 0.1 % for $T < 400$ K and 4 % for higher temperatures. Because of the restricted experimental data sets, no statement for the saturated liquid and vapour densities can be made. The uncertainty regarding the homogeneous density was assessed to be 0.05 % for $T < 320$ K and $p < 20$ MPa, whereas for higher temperatures and pressures uncertainties increase up to 0.5 %. The speed of sound can be calculated with an accuracy of 0.5 % at atmospheric pressure. The expected uncertainty of the isobaric heat capacity is 1 % in the gaseous and 0.2 % in the liquid

state. The physical and extrapolation behaviour of the equation of state was monitored carefully and found to be reasonable. Finally, the range of validity of the present equation was extended to $T_{max}$ = 1000 K and $p_{max}$ = 1200 MPa by means of molecular simulation data. Indications for possible uncertainties in this region are given, but cannot be verified because no experimental measurements are available.

Reference values to verify computer implementation, a fluid file for the application in the software packages REFPROP [125] and TREND [126], and the numerical values of the molecular simulation data are given in the supplementary material.

**Acknowledgements**

The authors gratefully acknowledge financial support by Deutsche Forschungsgemeinschaft under the grants VR6/4-2 and SP507/7-2. We would like to thank A. Kasischke for his assistance during the development of the equation of state and Dr. E. W. Lemmon for his support.

The simulations were carried out on the Cray XC40 (Hazel Hen) computer at the High Performance Computing Center Stuttgart (HLRS) and on the OCuLUS cluster of the Paderborn Center for Parallel Computing ($PC^2$).

**References**

[1] D.-Y. Peng and D.B. Robinson, Ind. Eng. Chem. Fundam. **15**, 59 (1976).

[2] O. Redlich and J.N.S. Kwong, Chem. Rev. **44**, 233 (1949).

[3] S.H. Huang and M. Radosz, Ind. Eng. Chem. Res. **29**, 2284 (1990).

[4] B. Saager, R. Hennenberg, and J. Fischer, Fluid Phase Equilib. **72**, 41 (1992).

[5] B. Saager and J. Fischer, Fluid Phase Equilib. **72**, 67 (1992).

[6] B.I. Lee and M.G. Kesler, AIChE J. **21**, 510 (1975).

[7] Römpp Encyclopedia Online: http://www.roempp.com (Thieme Verlag, Stuttgart, 2007, accessed at 10/11/2014.

[8] F. Amireche-Ziar, G. Boukais-Belaribi, A. Jakob, I. Mokbel, and F.B. Belaribi, Fluid Phase Equilib. **268**, 39 (2008).

[9] A. Barhala, D. Dragoescu, M. Teodorescu, and I. Wichterle, J. Chem. Thermodyn. **38**, 617 (2006).

[10] F. Comelli and R. Francesconi, J. Chem. Eng. Data **39**, 560 (1994).

[11] F. Comelli and R. Francesconi, J. Chem. Eng. Data **40**, 21 (1995).

[12] M. Comtat, M. Enjalbert, and J. Mahenc, Chim. Ind. Genie Chim. **102**, 225 (1969).

[13] W. Davies, J.B. Jaggeh, and H.K. Whalley, J. Chem. Technol. Biotechnol. **68**, 26 (1949).

[14] H.J. Dietrich, VDI-Forschungsheft **42**, 1 (1976).

[15] V. Dohnal, D. Bláhová, and R. Holub, Fluid Phase Equilib. **9**, 187 (1982).

[16] F. Garcia-Sanchez and A. Trejo, J. Chem. Thermodyn. **17**, 981 (1985).

[17] N.F. Giles and G.M. Wilson, J. Chem. Eng. Data **51**, 1973 (2006).

[18] B. Gutsche and H. Knapp, Fluid Phase Equilib. **8**, 285 (1982).

[19] O. Igoudjilene, A. Ait-Kaci, and J. Jose, Int. Electron J. Phys. Chem. Data **5**, 135 (1999).

[20] E. Kirschbaum, H. Fischer, and D. Wolf, Chem. Ing. Tech. **34**, 423 (1962).

[21] H. Kirss, M. Kuus, and E. Siimer, Proc. Est. Acad. Sci. **51**, 215 (2002).

[22] E.W. McGovern, Ind. Eng. Chem. **35**, 1230 (1943).

[23] G. Miksch, E. Liebermann, and F. Kohler, Monatsh. Chem. **100**, 1574 (1969).

[24] H.R. Patel, S. Sundaram, and D.S. Viswanath, J. Chem. Eng. Data **24**, 40 (1979).

[25] J.N. Pearce and P.E. Peters, J. Phys. Chem. **33**, 873 (1928).

[26] D. Radulescu and M. Alexa, Rom. J. Chem. **20**, 89 (1938).

[27] M.V. Rao and D.S. Viswanath, J. Chem. Eng. Data **27**, 41 (1982).

[28] F. Rivenq, Bull. Soc. Chim. Fr. **11**, 2429 (1974).

[29] A.P. Rollet, P. Toledano, G. Elkai, and M. Sénez, Publications scientifiques de l'Université d'Alger Sér. B403 (1956).

[30] P.A. Sewell and R. Stock, Trans. Faraday Soc. **67**, 1617 (1971).

[31] L. Sieg, J.L. Cruetzen, and W. Jost, Z. Phys. Chem. (Leipzig) **198**, 263 (1951).

[32] E.R. Smith and H. Matheson, J. Res. Nat. Bur. Stand. **20**, 641 (1938).

[33] D.R. Stull, Ind. Eng. Chem. **39**, 517 (1947).

[34] S. Sundaram and D.S. Viswanath, J. Chem. Eng. Data **21**, 448 (1976).

[35] M. Teodorescu, A. Barhala, and O. Landauer, Int. Electron J. Phys. Chem. Data **3**, 101 (1997).

[36] A.P. Toropov and Nikonovich, Zh. Fiz. Khim. **29**, 615 (1955).

[37] R.M. Varushchenko, S.S. Puchkov, and A.I. Druzhinina, Russ. J. Phys. Chem. **56**, 1805 (1982).

[38] J.A. Waters, G.A. Mortimer, and H.E. Clements, J. Chem. Eng. Data **15**, 174 (1970).

[39] W.V. Wilding, L.C. Wilson, and G.M. Wilson, Fluid Phase Equilib. **36**, 67 (1987).

[40] A. Ali and M. Tariq, J. Mol. Liq. **137**, 64 (2008).

[41] S.F. Babak and V.V. Udovenko, Russ. J. Gen. Chem. Russian **20**, 2199 (1950).

[42] B.H. Billings and D.E. Gray, *American Institute of Physics Handbook. Constants of Polyatomic Molecules, by G. Herzberg and L. Herzberg*, 3rd ed. (McGraw-Hill, New York, 1972).

[43] W. Herz and M. Levi, Z. Anorg. Allg. Chem. **183**, 340 (1929).

[44] S.S. Joshi, T.M. Aminabhavi, and S.S. Shukla, J. Chem. Eng. Data **35**, 247 (1990).

[45] C. Klofutar, Š. Paljk, and S. Golc-Teger, Thermochim. Acta **196**, 401 (1992).

[46] A. Kumagai and S. Takahashi, J. Chem. Thermodyn. **17**, 977 (1985).

[47] A.M. Martin, V.B. Rodríguez, and D.M. Villena, Afinidad **40**, 241 (1983).

[48] G. Sivaramprasad, M.V. Rao, and Prasad, D. H. L., J. Chem. Eng. Data **35**, 122 (1990).

[49] V.V. Udovenko, R.P. Airapetova, and R.I. Filatova, Russ. J. Gen. Chem. Russian **21**, 1559 (1951).

[50] R.M. Varushchenko, O.L. Vikhlakova, N.S. Mirzabekyants, S.S. Puchkov, and V.V. Galkina, Vestn. Mosk. Univ. Ser. 2 Khim **22**, 545 (1981).

[51] A.I. Vogel, J. Chem. Soc. **2**, 644 (1948).

[52] S.C. Bhatia, R. Bhatia, and G.P. Dubey, J. Chem. Thermodyn. **42**, 114 (2010).

[53] O. Ciocirlan, M. Teodorescu, D. Dragoescu, O. Iulian, and A. Barhala, J. Chem. Eng. Data **55**, 968 (2010).

[54] R.J. Fort and W.R. Moore, Trans. Faraday Soc. **61**, 2102 (1965).

[55] P. García-Giménez, J.F. Martínez-López, S.T. Blanco, I. Velasco, and S. Otín, J. Chem. Eng. Data **52**, 2368 (2007).

[56] G. Hahn, P. Svejda, and A. Dallos, Fluid Phase Equilib. **86**, 293 (1993).

[57] R.T. Lagemann, D.R. McMillan, and W.E. Woolf, J. Chem. Phys. **17**, 369 (1949).

[58] R. Malhotra, W.E. Price, L.A. Woolf, and A.J. Easteal, Int. J. Thermophys. **11**, 835 (1990).

[59] R. Malhotra and L.A. Woolf, Fluid Phase Equilib. **95**, 227 (1994).

[60] M. Manfredini, A. Marchetti, S. Sighinolfi, L. Tassi, A. Ulrici, and M. Vignali, J. Mol. Liq. **100**, 163 (2002).

[61] S.L. Oswal, B.M. Patel, A.M. Patel, and N.Y. Ghael, Fluid Phase Equilib. **206**, 313 (2003).

[62] S. Ranjbar, K. Fakhri, and J.B. Ghasemi, J. Chem. Eng. Data **54**, 3284 (2009).

[63] W. Schaaffs, Z. Phys. Chem. **194**, 28 (1944).

[64] A. Valtz, C. Coquelet, G. Boukais-Belaribi, A. Dahmani, and F.B. Belaribi, J. Chem. Eng. Data **56**, 1629 (2011).

[65] H. Iloukhani and B. Samiey, Phys. Chem. Liq. **45**, 571 (2007).

[66] J. Nath, J. Chem. Thermodyn. **28**, 481 (1996).

[67] J. Nath and A.P. Dixit, J. Chem. Eng. Data **29**, 313 (1984).

[68] J. Nath and R. Saini, J. Chem. Soc. Faraday Trans. **86**, 645 (1990).

[69] J. Nath and G. Singh, J. Chem. Eng. Data **31**, 327 (1986).

[70] G.C. Sekhar, P. Venkatesu, and Rao, Murari Venkata Prabhakara, J. Chem. Eng. Data **46**, 377 (2001).

[71] P. Góralski, M. Tkaczyk, and M. Chorążewski, J. Chem. Eng. Data **48**, 492 (2003).

[72] W.D. Gwinn and K.S. Pitzer, J. Chem. Phys. **16**, 303 (1948).

[73] D. Hallén, J. Chem. Thermodyn. **25**, 519 (1993).

[74] Y.L. Rastorguev and Y.A. Ganiev, Izv. Vyssh. Uchebn. Zaved., Neft Gaz **10**, 79 (1967).

[75] I. Shehatta, Thermochim. Acta **213**, 1 (1993).

[76] E. Wilhelm, J.-P. Grolier, and M. Ghassemi, Thermochim. Acta **28**, 59 (1979).

[77] A.S. Carson, P.G. Laye, J.B. Pedley, A.M. Welsby, J.S. Chickos, and S. Hosseini, J. Chem. Thermodyn. **26**, 1103 (1994).

[78] V. Majer, L. Šváb, and V. Svoboda, J. Chem. Thermodyn. **12**, 843 (1980).

[79] K. Bohmhammel and W. Mannchen, Z. Phys. Chem. **248**, 230 (1971).

[80] Y.J. Rao and D.S. Viswanath, J. Chem. Eng. Data **18**, 49 (1973).

[81] A.R. Paniego, Lluna, J. A. Burriel, and Garcia, J. E. Herrero, An. Quim. **70**, 349 (1975).

[82] P.J. Mohr, B.N. Taylor, and D.B. Newell, Rev. Mod. Phys. **84**, 1527 (2012).

[83] M.E. Wieser and M. Berglund, Pure Appl. Chem. **81**, 2131 (2009).

[84] R. Span, *Multiparameter Equations of State*. *An Accurate Source of Thermodynamic Property Data* (Springer, Berlin, 2000).

[85] K.S. Pitzer, J. Am. Chem. Soc. **63**, 2413 (1941).

[86] K.S. Pitzer and W.D. Gwinn, J. Am. Chem. Soc. **63**, 3313 (1941).

[87] R. Spitzer and K.S. Pitzer, J. Am. Chem. Soc. **68**, 2537 (1946).

[88] Y. Zhou, J. Liu, S.G. Penoncello, and E.W. Lemmon, J. Phys. Chem. Ref. Data **43**, 043105 (2014).

[89] H. Gedanitz, M.J. Dávila, and E.W. Lemmon, J. Chem. Eng. Data **60**, 1331 (2015).

[90] E.W. Lemmon (private communication).

[91] E.W. Lemmon and R.T. Jacobsen, J. Phys. Chem. Ref. Data **34**, 69 (2005).

[92] M. Frenkel, R.D. Chirico, V. Diky, K. Kroenlein, C.D. Muzny, A.F. Kazakov, J.W. Magee, I.M. Abdulagatov, and E.W. Lemmon, *NIST Standard Reference Database 103b: NIST Thermo-Data-Engine - Pure Components, Binary Mixtures, Reactions, Version 8.0* (National Institute of Standards and Technology, Gaithersburg, USA, 2013).

[93] R.L. Rowley, W.V. Wilding, J. Oscarson, Y. Yang, N. Zuendel, T. Daubert, and R. Danner, *DIPPR Data Compilation of Pure Chemical Properties* (Taylor & Francis Publishing Company, New York, 2004).

[94] A. Blondel-Telouk, H. Loiseleur, A. Barreau, E. Behar, and J. Jose, Fluid Phase Equilib. **110**, 315 (1995).

[95] L. Boublíková and B.C.-Y. Lu, J. Appl. Chem. **19**, 89 (1969).

[96] M. Thol, F.H. Dubberke, G. Rutkai, T. Windmann, A. Köster, R. Span, and J. Vrabec, Fluid Phase Equilib. **418**, 133 (2016).

[97] M. Thol, G. Rutkai, A. Köster, M. Kortmann, R. Span, and J. Vrabec, Chem. Eng. Sci. **121**, 87 (2015), **134**, 887–890 (2015).

[98] D. Ambrose, J. Sci. Instrum. **40**, 129 (1963).

[99] I.A. McLure and E. Dickinson, J. Chem. Thermodyn. **8**, 93 (1976).

[100] D. Ambrose, *Vapour-Liquid Critical Properties* (Teddington U.K.

[101] M. Thol, E.W. Lemmon, and R. Span, High Temp.-High Press. **41**, 81 (2012).

[102] J.A. Zollweg and G.W. Mulholland, J. Chem. Phys. **57**, 1021 (1972).

[103] E.W. Lemmon (private communication).

[104] D.R. McMillan, J. Acoust. Soc. Am. **19**, 956 (1947).

[105] S. Herrig, Master thesis, Ruhr-Universität Bochum 2013.

[106] L. Becker, O. Aufderhaar, and J. Gmehling, J. Chem. Eng. Data **45**, 661 (2000).

[107] W. Wagner and A. Pruss, J. Phys. Chem. Ref. Data **31**, 387 (2002).

[108] E.W. Lemmon and R. Span, J. Chem. Eng. Data **51**, 785 (2006).

[109] M. Thol, G. Rutkai, A. Köster, F.H. Dubberke, T. Windmann, R. Span, and J. Vrabec, J. Chem. Eng. Data **61**, 2580 (2016).

[110] M.P. Allen and D.J. Tildesley, *Computer Simulation of Liquids* (Clarendon Press, Oxford, 1987).

[111] C.G. Gray and K.E. Gubbins, *Theory of Molecular Fluids* (Clarendon Press, Oxford, 1984).

[112] J. Vrabec, J. Stoll, and H. Hasse, J. Phys. Chem. B **105**, 12126 (2001).

[113] R. Lustig, Molecular Physics **65**, 175 (1988).

[114] R. Lustig, Mol. Phys. **110**, 3041 (2012).

[115] J. Vrabec and H. Hasse, Mol. Phys. **100**, 3375 (2002).

[116] M. Thol, G. Rutkai, A. Köster, R. Span, J. Vrabec, and R. Lustig, J. Phys. Chem. Ref. Data **45**, 023101 (2016).

[117] I. Nezbeda and J. Kolafa, Mol. Sim. **5**, 391 (1991).

[118] J. Vrabec, M. Kettler, and H. Hasse, Chem. Phys. Lett. **356**, 431 (2002).

[119] C.W. Glass, S. Reiser, G. Rutkai, S. Deublein, A. Köster, G. Guevara-Carrion, A. Wafai, M. Horsch, M. Bernreuther, T. Windmann, H. Hasse, and J. Vrabec, Comp. Phys. Commun. **185**, 3302 (2014).

[120] G. Venkatarathnam and L.R. Oellrich, Fluid Phase Equilib. **301**, 225 (2011).

[121] K. Gao, J. Wu, P. Zhang, and E.W. Lemmon, J. Chem. Eng. Data **61**, 2859 (2016).

[122] R. Span and W. Wagner, Int. J. Thermophys. **18**, 1415 (1997).

[123] M. Thol, G. Rutkai, R. Span, J. Vrabec, and R. Lustig, Int. J. Thermophys. **36**, 25 (2015).

[124] V. Arp, J.M. Persichetti, and G.-b. Chen, J. Fluids Eng. **106**, 193 (1984).

[125] E.W. Lemmon, M.L. Huber, and M.O. McLinden, *NIST Standard Reference Database 23: Reference Fluid Thermodynamic and Transport Properties-REFPROP, Version 9.1* (National Institute of Standards and Technology, Gaithersburg, USA, 2013).

[126] R. Span, T. Eckermann, S. Herrig, S. Hielscher, A. Jäger, and M. Thol, *TREND. Thermodynamic Reference and Engineering Data 2.0* (Lehrstuhl für Thermodynamik, Ruhr-Universität Bochum, Bochum, Germany, 2015).

Table 1. Parameters of the residual contribution to the present equation of state, cf. Eq. (5).

| $i$ | $n_i$ | $t_i$ | $d_i$ | $p_i$ | $\eta_i$ | $\beta_i$ | $\gamma_i$ | $\varepsilon_i$ |
|---|---|---|---|---|---|---|---|---|
| 1 | $0.51000000 \cdot 10^{-1}$ | 1.000 | 4 | | | | | |
| 2 | $0.19900000 \cdot 10^{+1}$ | 0.352 | 1 | | | | | |
| 3 | $-0.25950000 \cdot 10^{+1}$ | 0.890 | 1 | | | | | |
| 4 | $-0.66530000 \cdot 10^{+0}$ | 0.824 | 2 | | | | | |
| 5 | $0.23595000 \cdot 10^{+0}$ | 0.498 | 3 | | | | | |
| 6 | $-0.17000000 \cdot 10^{+1}$ | 1.630 | 1 | 2 | | | | |
| 7 | $-0.44530000 \cdot 10^{+0}$ | 4.070 | 3 | 2 | | | | |
| 8 | $0.67247400 \cdot 10^{+0}$ | 0.679 | 2 | 1 | | | | |
| 9 | $-0.21918000 \cdot 10^{+0}$ | 2.850 | 2 | 2 | | | | |
| 10 | $-0.35540000 \cdot 10^{-1}$ | 1.070 | 7 | 1 | | | | |
| 11 | $0.97650000 \cdot 10^{+0}$ | 1.700 | 1 | - | 0.660 | 0.574 | 0.995 | 0.571 |
| 12 | $-0.49517900 \cdot 10^{+0}$ | 2.090 | 1 | - | 1.360 | 1.800 | 0.329 | 0.862 |
| 13 | $-0.23291174 \cdot 10^{+0}$ | 1.930 | 3 | - | 0.711 | 0.462 | 0.525 | 0.597 |
| 14 | $-0.10902450 \cdot 10^{-1}$ | 3.720 | 3 | - | 1.700 | 3.220 | 0.850 | 1.160 |
| 15 | $0.39209000 \cdot 10^{+0}$ | 1.580 | 1 | - | 1.110 | 2.220 | 0.585 | 0.208 |

Table 2. Average absolute relative deviations of experimental vapour pressure, saturated liquid, and saturated vapour densities calculated from the present equation of state. All temperatures were adapted to the ITS-90 scale. Data sets, which were applied to the fit, are marked with an asterisk.

| **Authors** | **No. of data** | **Temperature range / K** | **Average absolute relative deviations (*AAD*) / %** | | | |
|---|---|---|---|---|---|---|
| | | | **LT[a]** | **MT[a]** | **HT[a]** | **overall** |
| **Vapor pressure $p_v$** | | | | | | |
| Amireche-Ziar *et al*. [8]* | 20 | 284 - 355 | 0.080 | 1.14 | - | 0.50 |
| Barhala *et al*. [9] | 10 | 292 - 314 | 0.62 | - | - | 0.62 |
| Comelli & Francesconi [10] | 3 | 298 - 334 | 0.74 | - | - | 0.74 |
| Comelli & Francesconi [11] | 15 | 292 - 356 | 9.87 | 2.34 | - | 5.85 |
| Comtat *et al*. [12] | 14 | 326 - 355 | 2.96 | 4.24 | - | 3.78 |
| Davies *et al*. [13] | 4 | 293 - 324 | 0.78 | - | - | 0.78 |
| Dietrich [14] | 58 | 284 - 353 | 0.17 | 0.19 | - | 0.17 |
| Dohnal *et al*. [15] | 15 | 324 - 355 | 0.022 | 0.021 | - | 0.021 |
| Garcia-Sanchez & Trejo [16] | 65 | 351 - 547 | - | 2.15 | - | 2.15 |
| Giles & Wilson [17] | 2 | 303 - 354 | 0.055 | 0.25 | - | 0.15 |

| Authors | No. of data | Temperature range / K | Average absolute relative deviations (*AAD*) / % LT[a] | MT[a] | HT[a] | overall |
|---|---|---|---|---|---|---|
| Gutsche & Knapp [18] | 15 | 301 - 358 | 0.12 | 0.099 | - | 0.12 |
| Igoudjilene *et al*. [19] | 10 | 263 - 344 | 0.43 | 0.40 | - | 0.43 |
| Kirschbaum *et al*. [20] | 2 | 356 - 362 | - | 0.46 | - | 0.46 |
| Kirss *et al*. [21] | 4 | 319 - 357 | 0.19 | 0.042 | - | 0.079 |
| McGovern [22] | 1 | 356.62 | - | 0.084 | - | 0.084 |
| Miksch *et al*. [23] | 3 | 286 - 306 | 3.36 | - | - | 3.36 |
| Patel *et al*. [24] | 16 | 343 - 382 | - | 0.55 | - | 0.55 |
| Pearce & Peters [25] | 27 | 242 - 373 | 2.45 | 1.01 | - | 2.02 |
| Radulescu & Alexa [26] | 6 | 273 - 299 | 1.10 | - | - | 1.10 |
| Rao & Viswanath [27]* | 59 | 344 - 404 | - | 2.01 | 2.57 | 2.46 |
| Rivenq [28] | 5 | 318 - 356 | 1.55 | 2.11 | - | 1.89 |
| Rollet *et al*. [29] | 18 | 353 - 385 | - | 0.21 | - | 0.21 |
| Sewell & Stock [30] | 6 | 273 - 324 | 0.80 | - | - | 0.80 |
| Sieg *et al*. [31] | 1 | 356.61 | - | 0.13 | - | 0.13 |
| Smith & Matheson [32] | 17 | 352 - 361 | - | 0.17 | - | 0.17 |
| Stull [33] | 18 | 228 - 559 | 19.1 | 4.71 | 1.61 | 11.0 |
| Sundaram & Viswanath [34] | 20 | 343 - 382 | - | 0.64 | - | 0.64 |
| Teodorescu *et al*. [35] | 2 | 323 - 354 | 0.15 | 0.092 | - | 0.12 |
| Toropov & Nikonovich [36] | 3 | 313 - 334 | 0.77 | - | - | 0.77 |
| Varushchenko *et al*. [37] | 15 | 298 - 357 | 0.083 | 0.077 | - | 0.080 |
| Waters *et al*. [38] | 5 | 263 - 299 | 0.82 | - | - | 0.82 |
| Wilding *et al*. [39] | 2 | 243 - 274 | 4.18 | - | - | 4.18 |
| **Saturated liquid density $\rho'$** | | | | | | |
| Ali & Tariq [40] | 5 | 298 - 319 | 0.19 | - | - | 0.19 |
| Babak & Udovenko [41] | 3 | 298 - 349 | 0.21 | 0.23 | - | 0.22 |
| Comelli & Francesconi [10] | 1 | 298.15 | 0.025 | - | - | 0.025 |
| Herz & Levi [43] | 4 | 293 - 324 | 0.13 | - | - | 0.13 |
| Joshi *et al*. [44] | 4 | 298 - 314 | 0.015 | - | - | 0.015 |
| Klofutar *et al*. [45] | 6 | 293 - 334 | 0.066 | - | - | 0.066 |
| Kumagai & Takahashi [46] | 5 | 298 - 399 | 0.073 | 0.29 | - | 0.20 |
| Martin *et al*. [47] | 5 | 303 - 344 | 0.46 | 0.41 | - | 0.45 |
| Sivaramprasad *et al*. [48] | 5 | 293 - 334 | 0.26 | - | - | 0.26 |
| Udovenko *et al*. [49] | 4 | 303 - 334 | 0.27 | - | - | 0.27 |
| Varushchenko *et al*. [50] | 6 | 293 - 334 | 0.036 | - | - | 0.036 |
| Vogel [51] | 5 | 286 - 334 | 0.16 | - | - | 0.16 |
| **Saturated vapor density $\rho''$** | | | | | | |
| McGovern [22] | 1 | 356.62 | - | 3.03 | - | 3.03 |

[a] LT: $T/T_c < 0.6$; MT: $0.6 \le T/T_c \le 0.98$; HT: $T/T_c > 0.98$

Table 3. Parameters for the ancillary equations, cf. Eqs. (8) to (10).

| | $p_v$: Eq. (8) | | $\rho'$: Eq. (9) | | $\rho''$: Eq. (10) | |
|---|---|---|---|---|---|---|
| $i$ | $n_i$ | $t_i$ | $n_i$ | $t_i$ | $n_i$ | $t_i$ |
| 1 | $-0.898372 \cdot 10^{+1}$ | 1.00 | $0.170532 \cdot 10^{+1}$ | 0.30 | $-0.293901 \cdot 10^{+1}$ | 0.37 |
| 2 | $0.154600 \cdot 10^{+2}$ | 1.50 | $0.178600 \cdot 10^{+0}$ | 0.70 | $-0.645628 \cdot 10^{+1}$ | 1.20 |
| 3 | $-0.371100 \cdot 10^{+2}$ | 1.90 | $0.147900 \cdot 10^{+1}$ | 1.10 | $-0.497300 \cdot 10^{+2}$ | 3.50 |
| 4 | $0.408520 \cdot 10^{+2}$ | 2.30 | $-0.622480 \cdot 10^{+0}$ | 1.50 | $0.732730 \cdot 10^{+2}$ | 4.30 |
| 5 | $-0.200420 \cdot 10^{+2}$ | 2.80 | | | $-0.837170 \cdot 10^{+2}$ | 5.40 |
| 6 | | | | | $-0.966800 \cdot 10^{+2}$ | 13.0 |

Table 4. Average absolute relative deviations of the experimental data of homogeneous states from the present equation of state. All temperatures were adapted to the ITS-90 scale. Data sets, which were applied to the fit, are marked with an asterisk. The values for the second virial coefficient are calculated as absolute deviations in $cm^3 \cdot mol^{-1}$.

| Authors | No. of data | Temperature and pressure range | | Average absolute relative deviation (*AAD*) / % | |
|---|---|---|---|---|---|
| | | $T$ / K | $p$ / MPa | Gas | Liquid |
| ***pρT* data** | | | | | |
| Bhatia *et al*. [52] | 2 | 293 - 314 | 0.101325 | | 0.012 |
| Ciocirlan *et al*. [53] | 4 | 288 - 319 | 0.101325 | | 0.010 |
| Fort & Moore [54] | 1 | 298.14 | 0.101325 | | 0.020 |
| García-Giménez *et al*. [55]* | 44 | 288 - 319 | 0.1 - 21 | | 0.010 |
| Hahn *et al*. [56] | 2 | 293 - 314 | 0.101325 | | 0.026 |
| Kumagai & Takahashi [46]* | 35 | 298 - 399 | 10 - 102 | | 0.19 |
| Lagemann *et al*. [57] | 4 | 293 - 324 | 0.101325 | | 0.029 |
| Malhotra *et al*. [58] | 4 | 278 - 339 | 0.101325 | | 0.042 |
| Malhotra & Woolf [59] | 6 | 278 - 339 | 0.101325 | | 0.042 |
| Manfredini *et al*. [60] | 17 | 263 - 344 | 0.101325 | | 0.043 |
| Oswal *et al*. [61] | 5 | 298 - 334 | 0.101325 | | 0.028 |
| Ranjbar *et al*. [62] | 6 | 288 - 314 | 0.101325 | | 0.082 |
| Schaaffs [63] | 1 | 293.14 | 0.101325 | | 0.028 |
| Valtz *et al*. [64] | 51 | 283 - 334 | 0.101325 | | 0.010 |
| **Speed of sound *w*** | | | | | |
| Ali & Tariq [40] | 5 | 298 - 319 | 0.101325 | | 0.65 |
| Bhatia *et al*. [52] | 2 | 293 - 314 | 0.101325 | | 0.074 |
| Fort & Moore [54] | 1 | 298.14 | 0.101325 | | 0.74 |
| Iloukhani & Samiey [65] | 1 | 303.15 | 0.101325 | | 0.55 |

| Authors | No. of data | Temperature and pressure range $T$ / K | $p$ / MPa | Average absolute relative deviation ($AAD$) / % Gas | Liquid |
|---|---|---|---|---|---|
| Lagemann *et al*. [57]* | 6 | 273 - 324 | 0.101325 | | 0.067 |
| Nath [66] | 1 | 303.15 | 0.101325 | | 0.095 |
| Nath & Dixit [67] | 2 | 298 - 309 | 0.101325 | | 0.053 |
| Nath & Saini [68] | 2 | 303 - 314 | 0.101325 | | 0.19 |
| Nath & Singh [69] | 2 | 303 - 314 | 0.101325 | | 0.060 |
| Oswal *et al*. [61] | 5 | 298 - 334 | 0.101325 | | 0.41 |
| Schaaffs [63] | 1 | 293.14 | 0.101325 | | 17.4 |
| Sekhar *et al*. [70] | 1 | 303.15 | 0.101325 | | 0.092 |
| **Isobaric heat capacity $c_p$** | | | | | |
| Góralski *et al*. [71]* | 30 | 284 - 354 | 0.101325 | | 0.097 |
| Gwinn & Pitzer [72] | 6 | 379 - 557 | 0.101325 | 0.26 | |
| Hallén [73] | 1 | 298.15 | 0.101325 | | 0.39 |
| Rastorguev & Ganiev [74] | 4 | 293 - 354 | 0.101325 | | 0.69 |
| Shehatta [75] | 2 | 298 - 309 | 0.101325 | | 0.36 |
| Sieg *et al*. [31] | 1 | 293.15 | 0.101325 | | 3.5 |
| Wilhelm *et al*. [76] | 1 | 298.15 | 0.101325 | | 0.27 |
| **Heat of vaporization $\Delta h_v$** | | | | | |
| Carson *et al*. [77] | 1 | 298.15 | $p_v$ | 2.0 | |
| Majer *et al*. [78] | 5 | 298 - 359 | $p_v$ | 0.21 | |
| McGovern [22] | 1 | 356.62 | $p_v$ | 0.27 | |
| Rao & Viswanath [80] | 2 | 353 - 357 | $p_v$ | 0.17 | |
| **Second virial coefficient $B$** | | | | | |
| Bohmhammel & Mannchen [79] | 12 | 364 - 579 | | 8.97 | |
| Paniego *et al*. [81] | 4 | 365 - 414 | | 221 | |
| Sewell & Stock [30] | 6 | 273 - 324 | | 2.69 | |

Table 5. Parameters of the present molecular interaction model for 1,2-dichloroethane. Lennard-Jones interaction sites are denoted by the modelled atoms or atomic groups. The electrostatic interaction site is denoted by quadrupole. Coordinates ($x$, $y$, $z$) are given with respect to the centre of mass in a principal axes system. The orientation of the quadrupole is defined in standard Euler angles, where $\varphi$ is the azimuthal angle with respect to the $x$-$z$ plane and $\theta$ is the inclination angle with respect to the $z$ axis. $k_B$ is the Boltzmann constant.

| Interaction site | $x$ / Å | $y$ / Å | $z$ / Å | $\sigma$ / Å | $\varepsilon \cdot k_B^{-1}$ / K | $\varphi$ / deg | $\theta$ / deg | $Q$ / $10^{-39}$ A m$^2$ s |
|---|---|---|---|---|---|---|---|---|
| Cl | −0.4757 | 2.1203 | 0 | 3.52 | 135 | | | |
| $CH_2$ | 0.4757 | 0.5904 | 0 | 3.76 | 76.95 | | | |
| $CH_2$ | −0.4757 | −0.5904 | 0 | 3.76 | 76.95 | | | |
| Cl | 0.4757 | −2.1203 | 0 | 3.52 | 135 | | | |
| Quadrupole | 0 | 0 | 0 | | | 60 | 90 | −2.9354 |

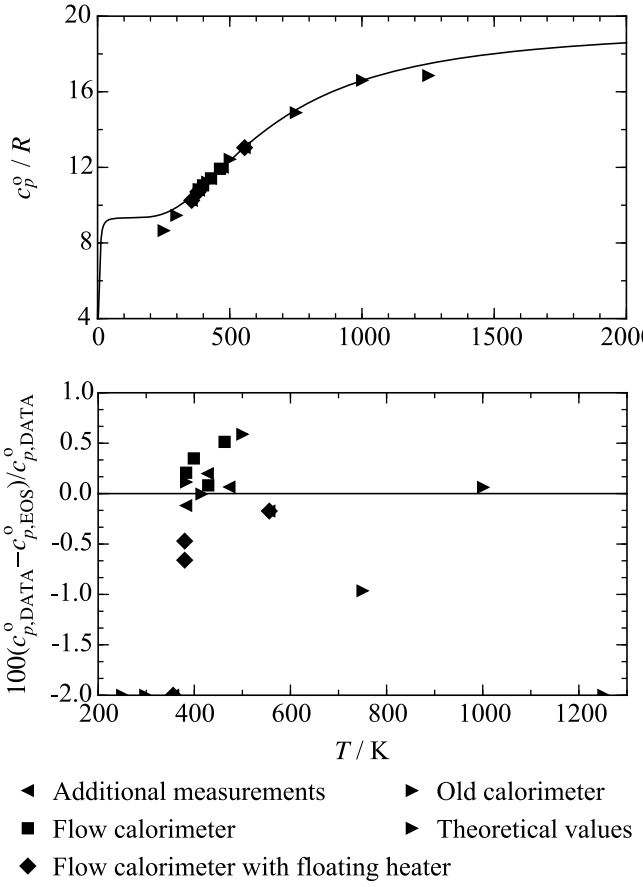


Figure 1. Representation of the isobaric heat capacity of the ideal gas of Gwinn and Pitzer [72].

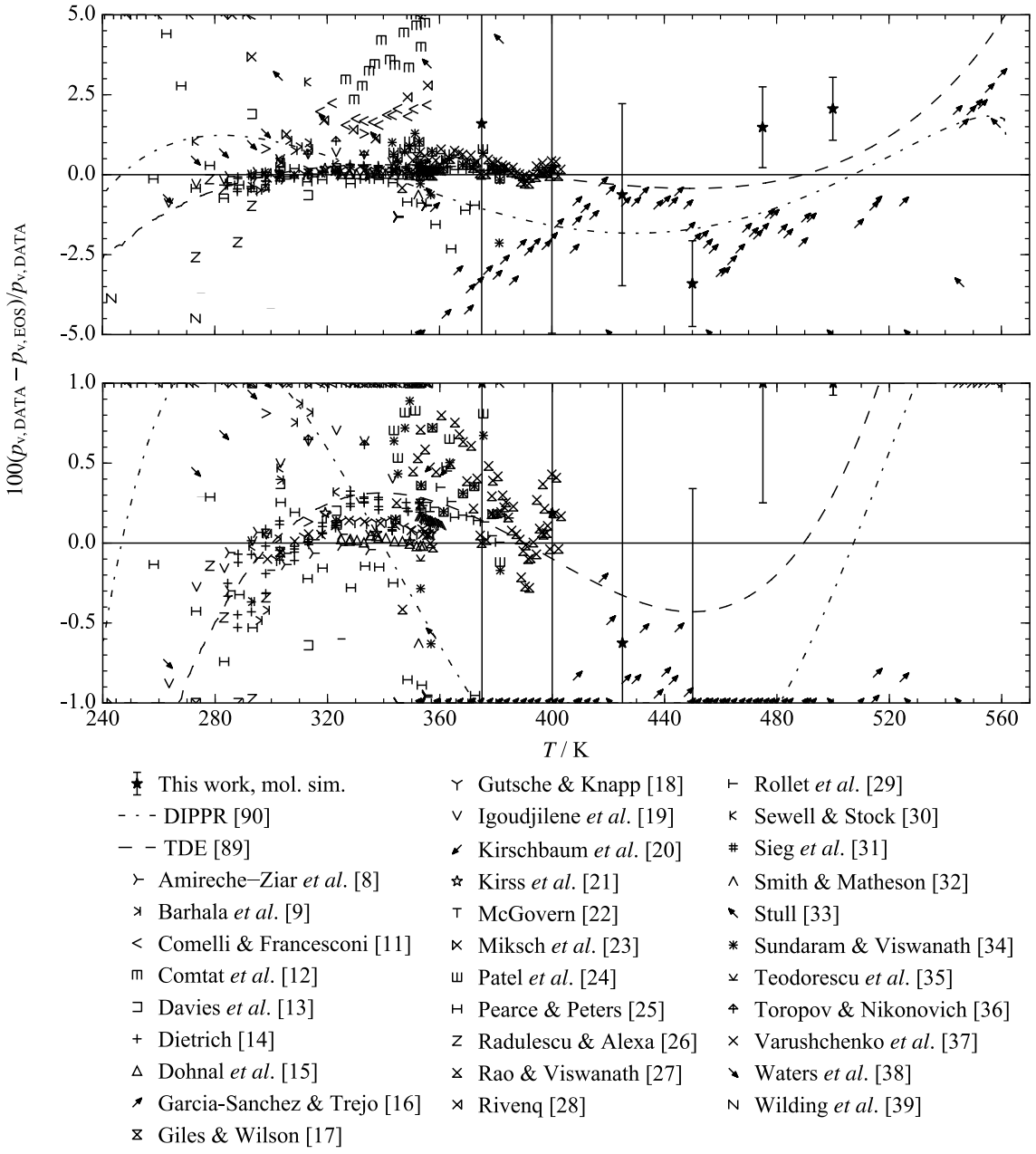


Figure 2. Relative deviations of vapour pressure data from the present equation of state.

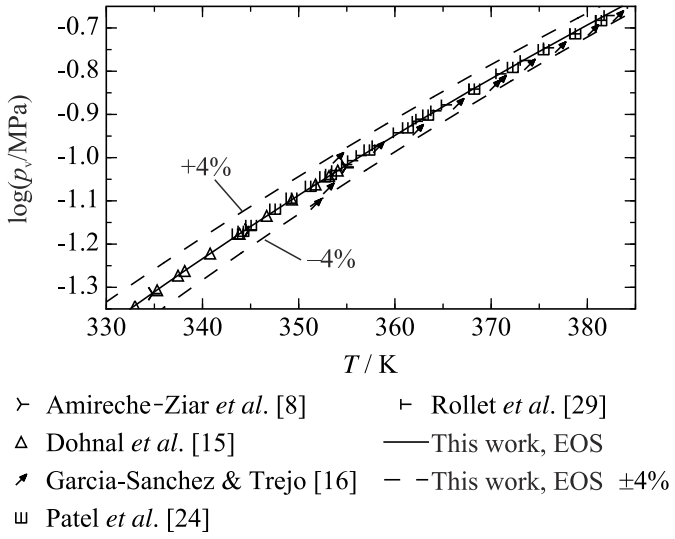


Figure 3. log($p_v$)-$T$ diagram including selected experimental vapour pressure data.

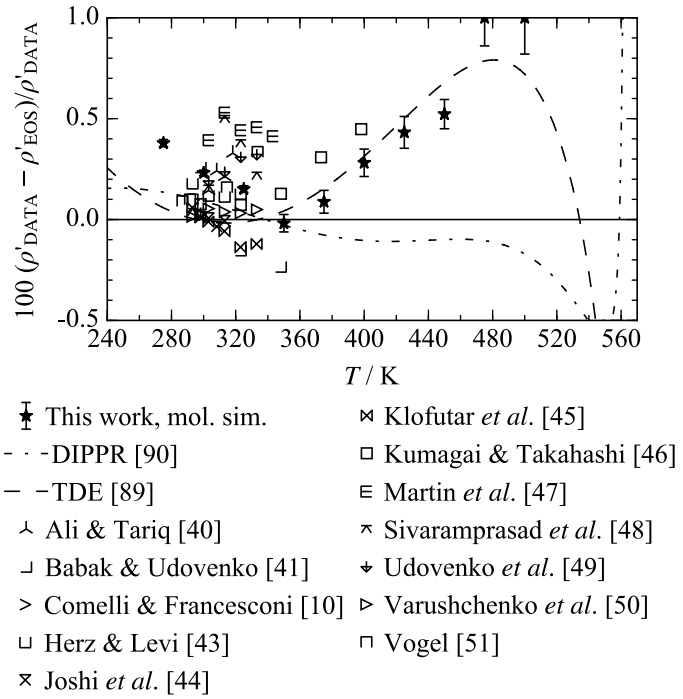


Figure 4. Relative deviations of saturated liquid density data from the present equation of state.

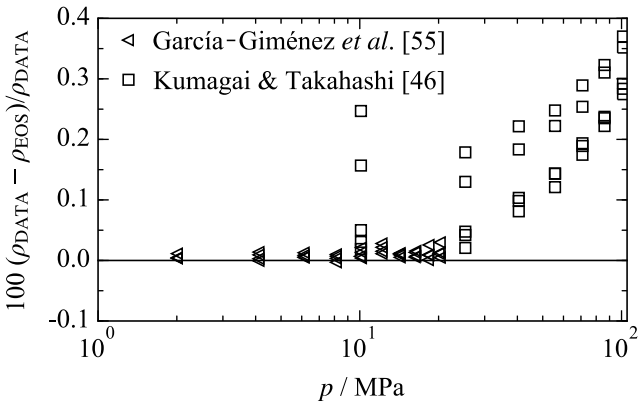


Figure 5. Relative deviations of experimental homogeneous density data from the present equation of state for 285 K < $T$ < 400 K.

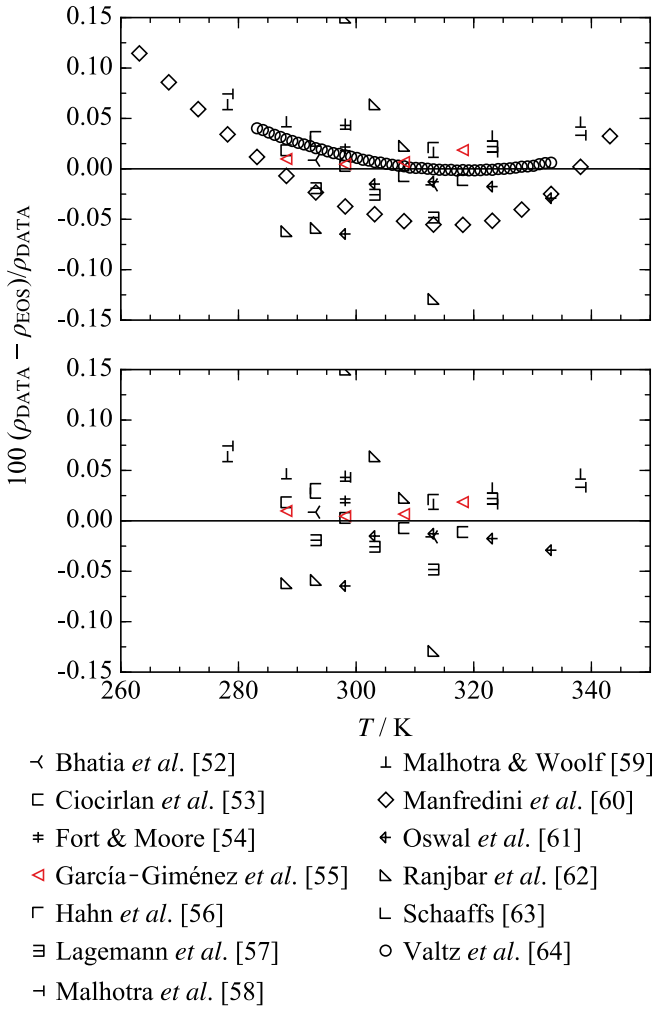


Figure 6. Relative deviations of experimental homogeneous density data from the present equation of state at atmospheric pressure.

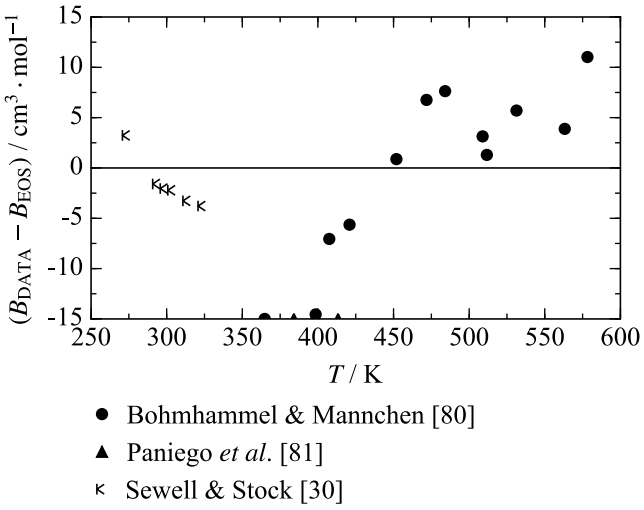


Figure 7. Absolute deviations of second virial coefficient data from the present equation of state.

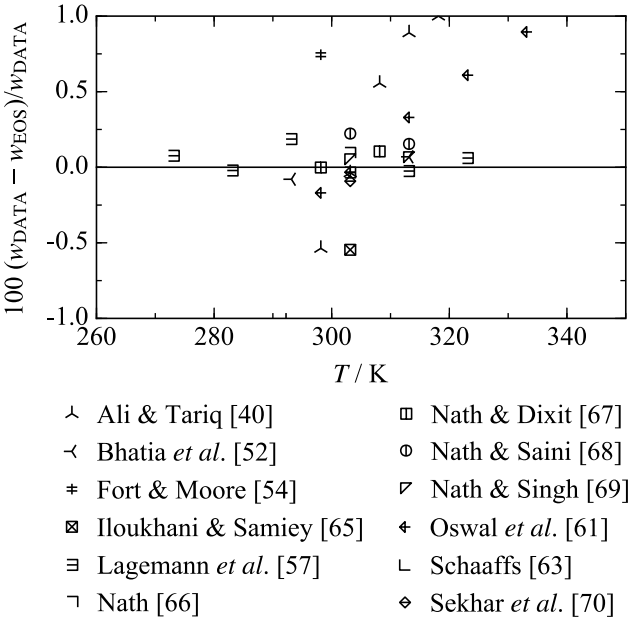


Figure 8. Relative deviations of experimental speed of sound data from the present equation of state at atmospheric pressure.

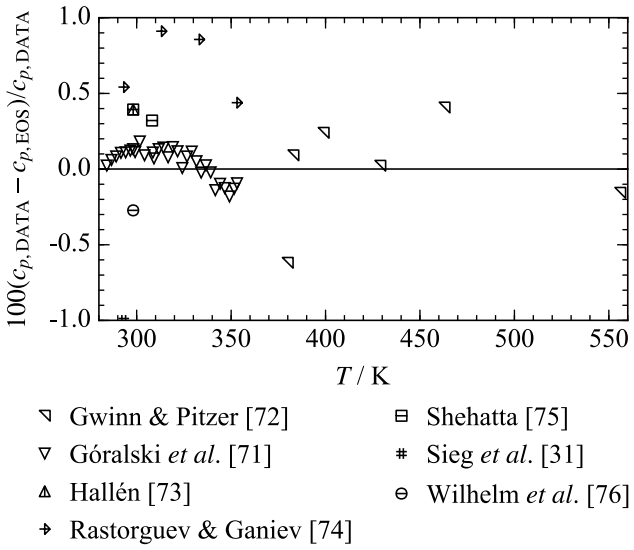


Figure 9. Relative deviations of experimental isobaric heat capacity data from the present equation of state at atmospheric pressure.

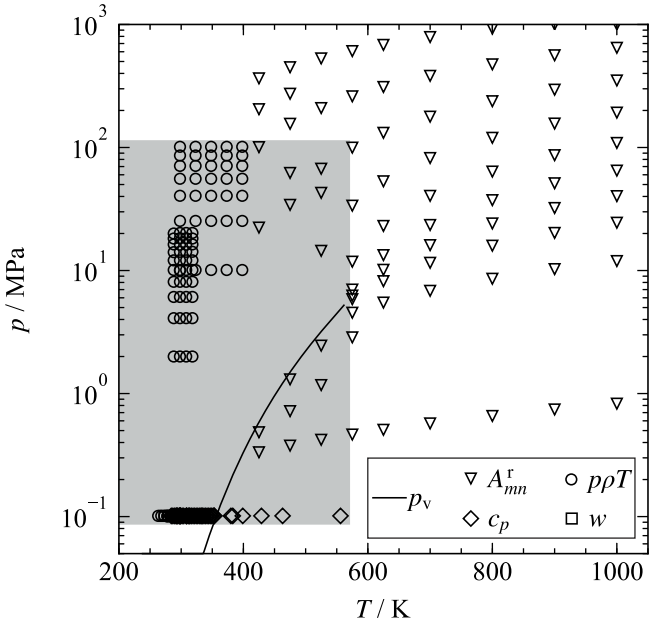


Figure 10. Available data for 1,2-dichloroethane in the homogeneous region. The grey area depicts the region where experimental data are available: $T_{max}$ = 560 K and $p_{max}$ = 100 MPa. The residual Helmholtz derivatives $A^{r}_{mn}$ from molecular simulation extend this region up to $T_{max}$ = 1000 K and $p_{max}$ = 1200 MPa.

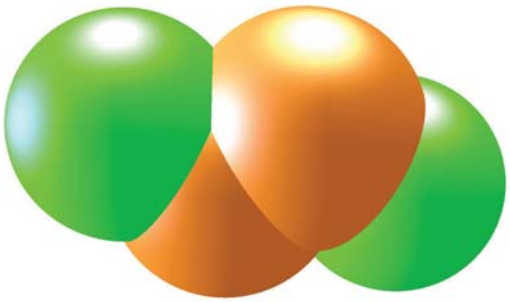

Figure 11. Present molecular interaction model for 1,2-dichloroethane. The green spheres represent chlorine atoms, the brown spheres represent methylene groups. Note that the sphere diameters correspond to the Lennard-Jones size parameters, which are depicted according to the molecular geometry scale.

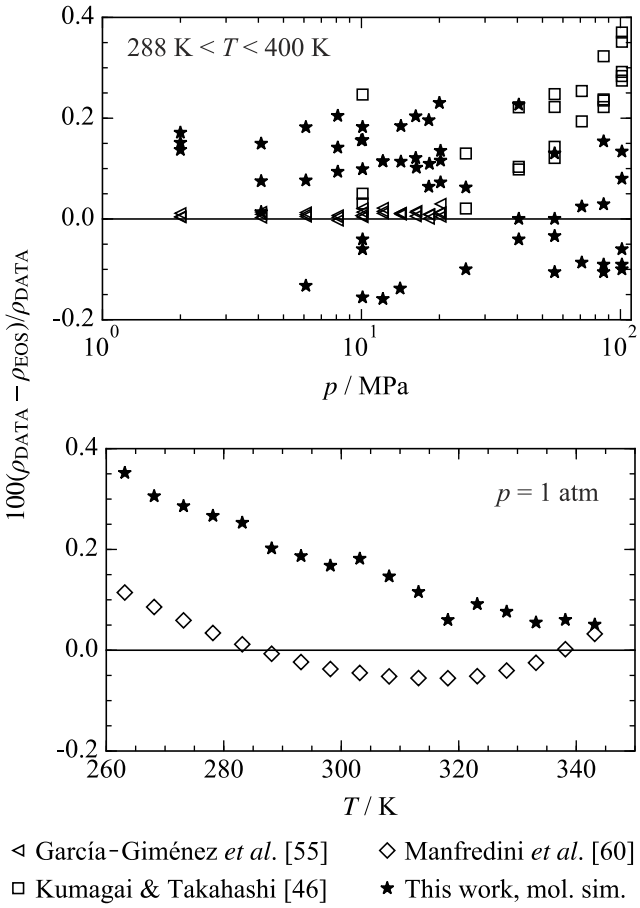


Figure 12. Relative deviations of experimental homogeneous density data from the present equation of state. At the same *p*-*T* state points, molecular simulation data are presented to verify the accuracy of the present molecular model.

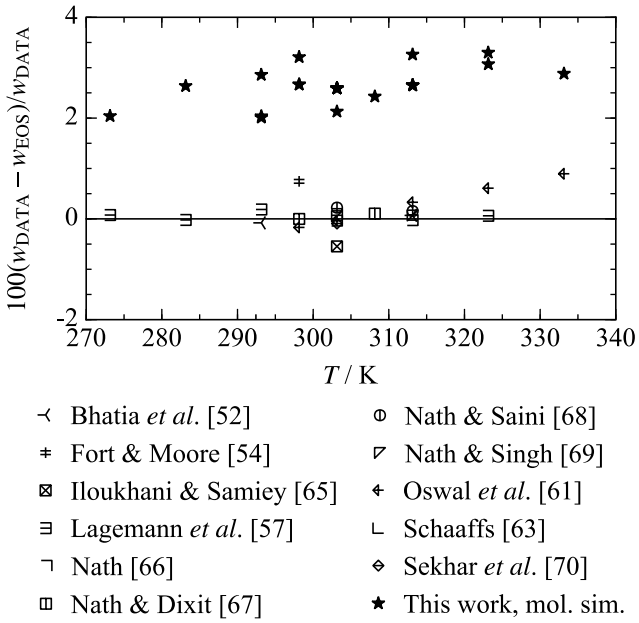


Figure 13. Relative deviations of experimental speed of sound data from the present equation of state at atmospheric pressure. At the same $p$-$T$ state points, molecular simulation data are presented to verify the accuracy of the molecular model.

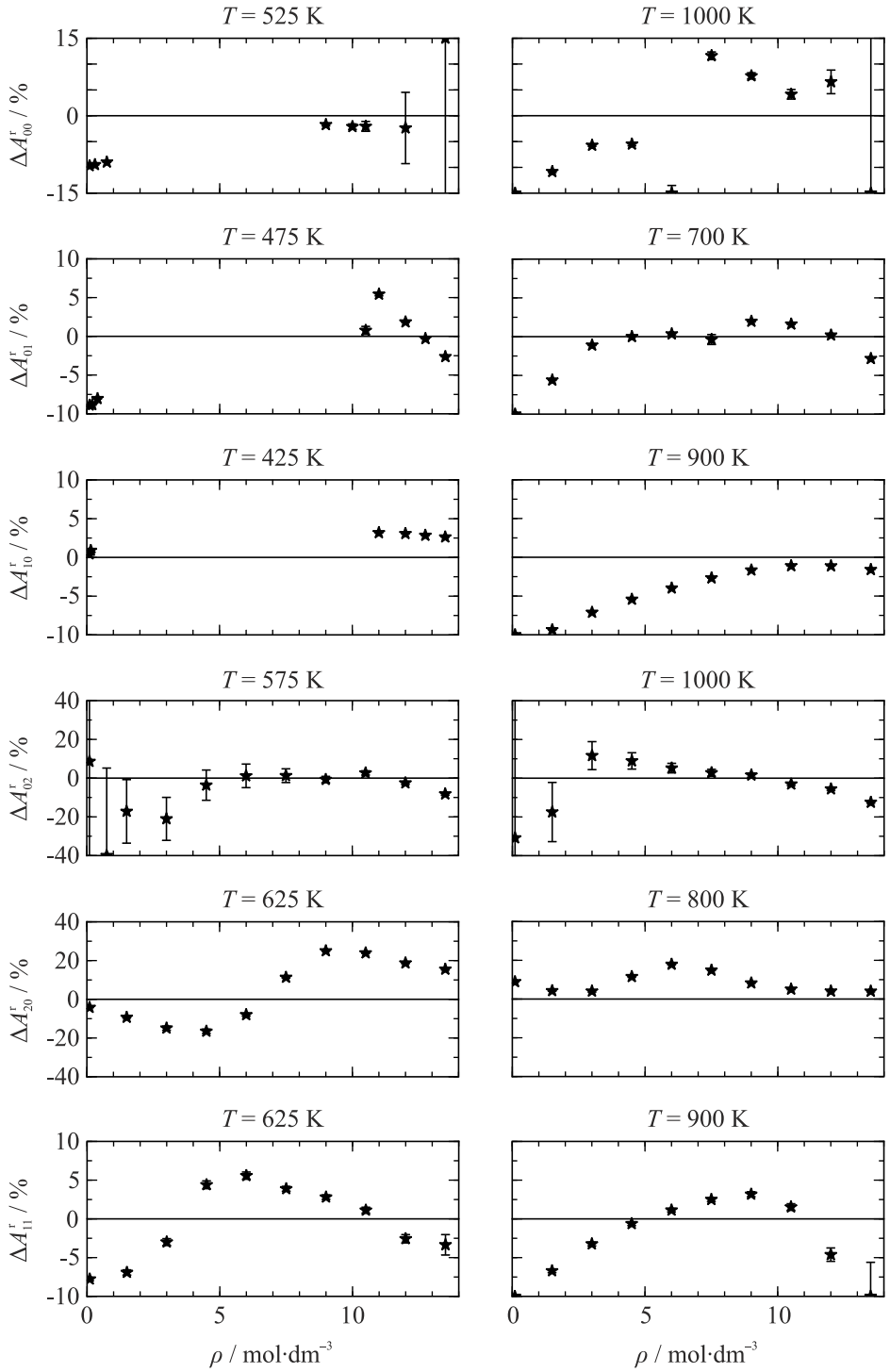


Figure 14. Relative deviations of simulated residual Helmholtz derivative data from the present equation of state along selected isotherms. Relative deviations are calculated according to Eq. (6).

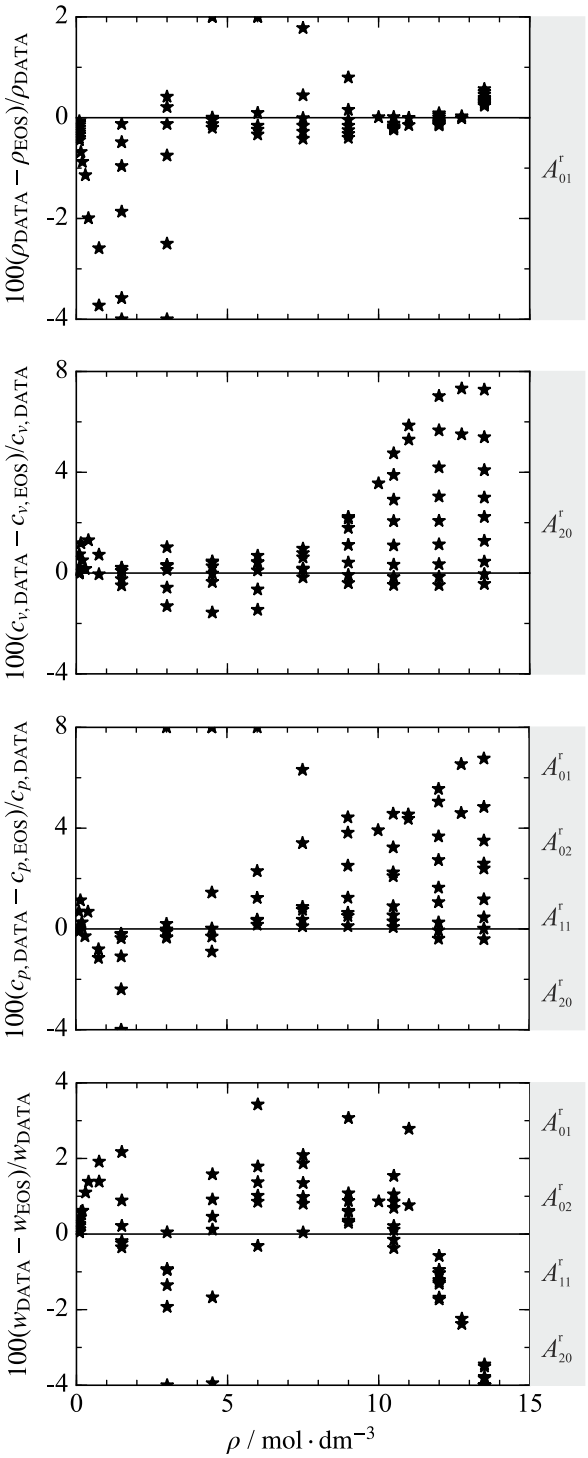


Figure 15. Comparison of the present equation of state with thermodynamic properties obtained from molecular simulation data ($T_{max}$ = 1000 K and $p_{max}$ = 1200 MPa). The involved residual Helmholtz energy derivatives are indicated in the grey boxes.

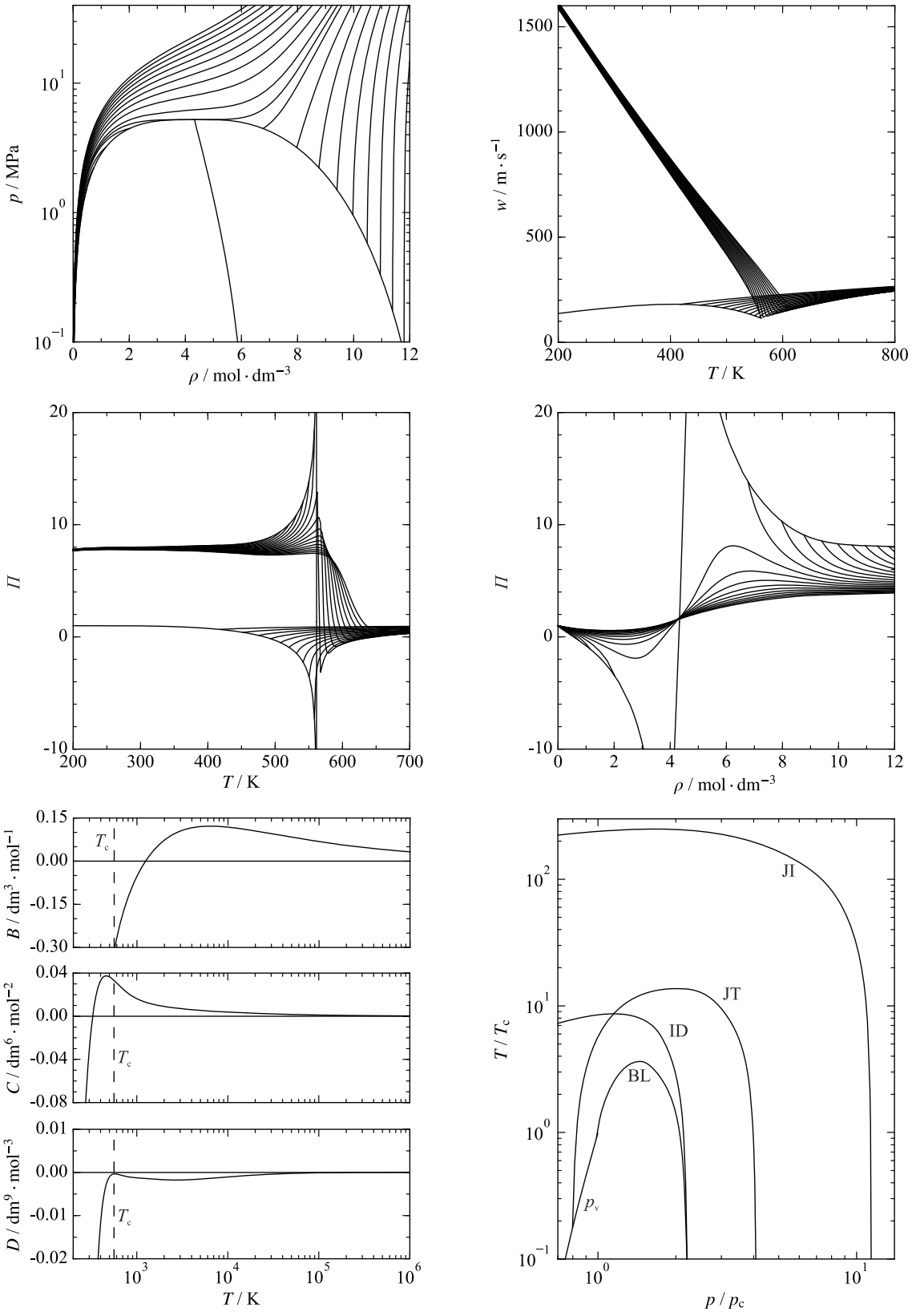


Figure 16. Physical behaviour of some thermodynamic properties of 1,2-dichloroethane: vapor-liquid equilibrium curves together with the rectilinear diameter (top left), speed of sound as a function of temperature along selected isobars (top right), phase

identification parameter as a function of temperature along selected isobars (center left), phase identification parameter as a function of density along selected isotherms (center right), second, third, and fourth virial coefficients (bottom left), and characteristic ideal curves [122] (bottom right). $p_v$: vapor pressure curve, BL: Boyle curve, ID: ideal curve, JT: Joule-Thomson inversion curve, JI: Joule inversion curve.

# Supporting information to the article:

## Equation of state for 1,2-dichloroethane based on a hybrid data set

Monika Thol[1*], Gabor Rutkai[2], Andreas Köster[2], Svetlana Miroshnichenko[2], Wolfgang Wagner[1], Jadran Vrabec[2], Roland Span[1]

[1]*Lehrstuhl für Thermodynamik, Ruhr-Universität Bochum, 44801 Bochum, Germany*

[2]*Lehrstuhl für Thermodynamik und Energietechnik, Universität Paderborn, 33098 Paderborn, Germany*

*Monika Thol, Lehrstuhl für Thermodynamik, Ruhr-Universität Bochum, Universitätsstraße 150, 44801 Bochum, Germany,

Phone: +49 234 32 26408

Fax: +49 234 32 14163

E-mail: m.thol@thermo.rub.de

Test values for computer implementation

| $T$ / K | $\rho$ / mol·dm$^{-3}$ | $p$ / MPa | $h$ / J·mol$^{-1}$ | $s$ / J·mol$^{-1}$·K$^{-1}$ | $c_p$ / J·mol$^{-1}$·K$^{-1}$ | $w$ / m·s$^{-1}$ | $a$ / J·mol$^{-1}$ |
|---|---|---|---|---|---|---|---|
| 250 | 0.0001 | $2.0782423 \cdot 10^{-4}$ | $2.3536919 \cdot 10^{+4}$ | $1.1263617 \cdot 10^{+2}$ | $7.9434919 \cdot 10^{+1}$ | $1.5314712 \cdot 10^{+2}$ | $-6.7003659 \cdot 10^{+3}$ |
| 250 | 14 | $1.3148464 \cdot 10^{+2}$ | $-6.3294127 \cdot 10^{+3}$ | $-5.4436721 \cdot 10^{+1}$ | $1.2357319 \cdot 10^{+2}$ | $1.7682675 \cdot 10^{+3}$ | $-2.1119925 \cdot 10^{+3}$ |
| 400 | 0.05 | $1.6082797 \cdot 10^{-1}$ | $3.5896016 \cdot 10^{+4}$ | $9.6321504 \cdot 10^{+1}$ | $9.3603168 \cdot 10^{+1}$ | $1.8706153 \cdot 10^{+2}$ | $-5.8491451 \cdot 10^{+3}$ |
| 400 | 12 | $7.2350760 \cdot 10^{+1}$ | $9.2143686 \cdot 10^{+3}$ | $8.2503437 \cdot 10^{+0}$ | $1.3062037 \cdot 10^{+2}$ | $1.1810220 \cdot 10^{+3}$ | $-1.1499891 \cdot 10^{+2}$ |
| 550 | 14 | $7.4415061 \cdot 10^{+2}$ | $6.8017209 \cdot 10^{+4}$ | $2.4569494 \cdot 10^{+1}$ | $1.3911233 \cdot 10^{+2}$ | $2.1697534 \cdot 10^{+3}$ | $1.3503729 \cdot 10^{+3}$ |

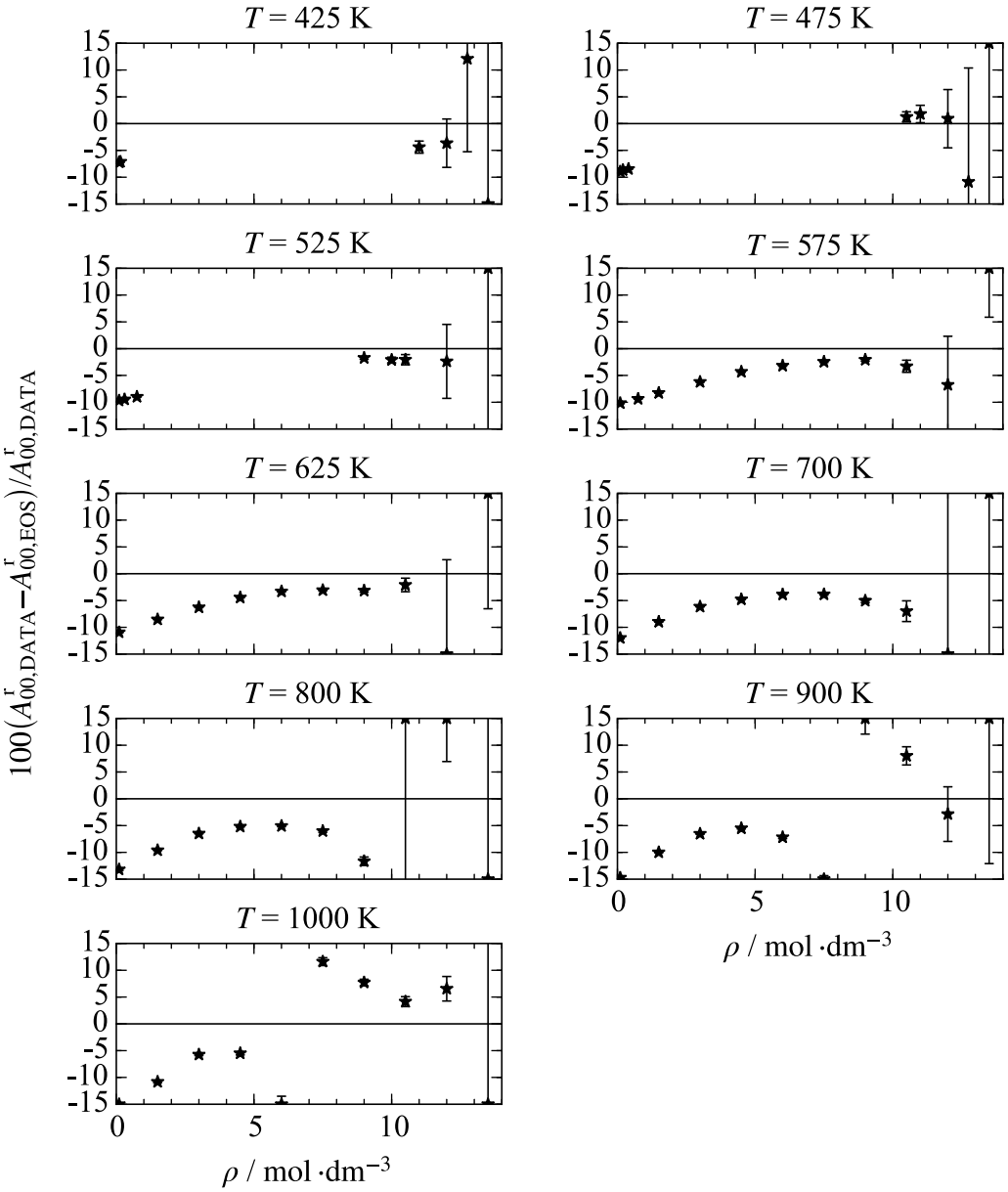


Figure S1. Relative deviation of simulated residual reduced Helmholtz energy data from the present equation of state.

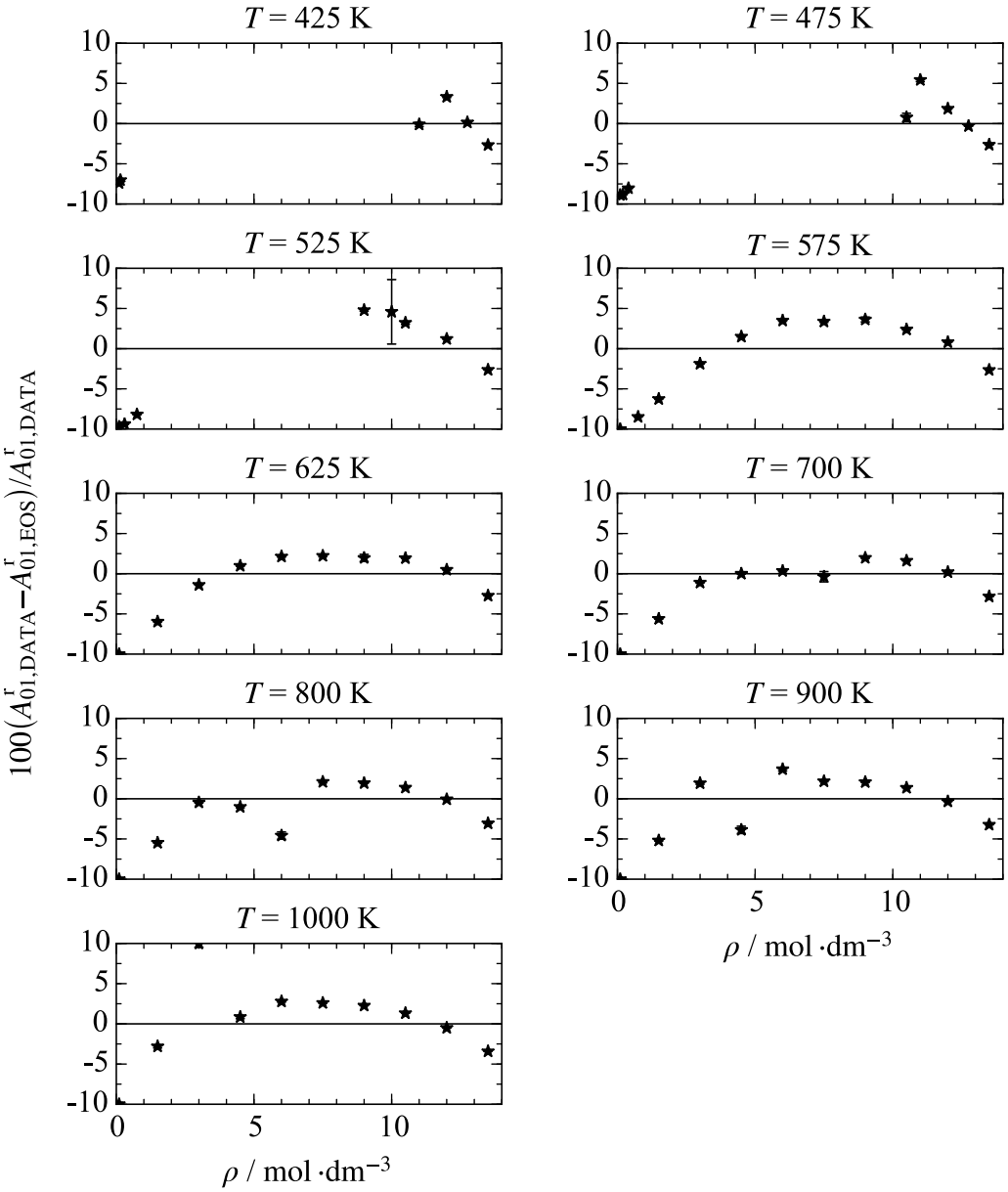


Figure S2. Relative deviation of simulated first derivative of the residual Helmholtz energy with respect to density data from the present equation of state.

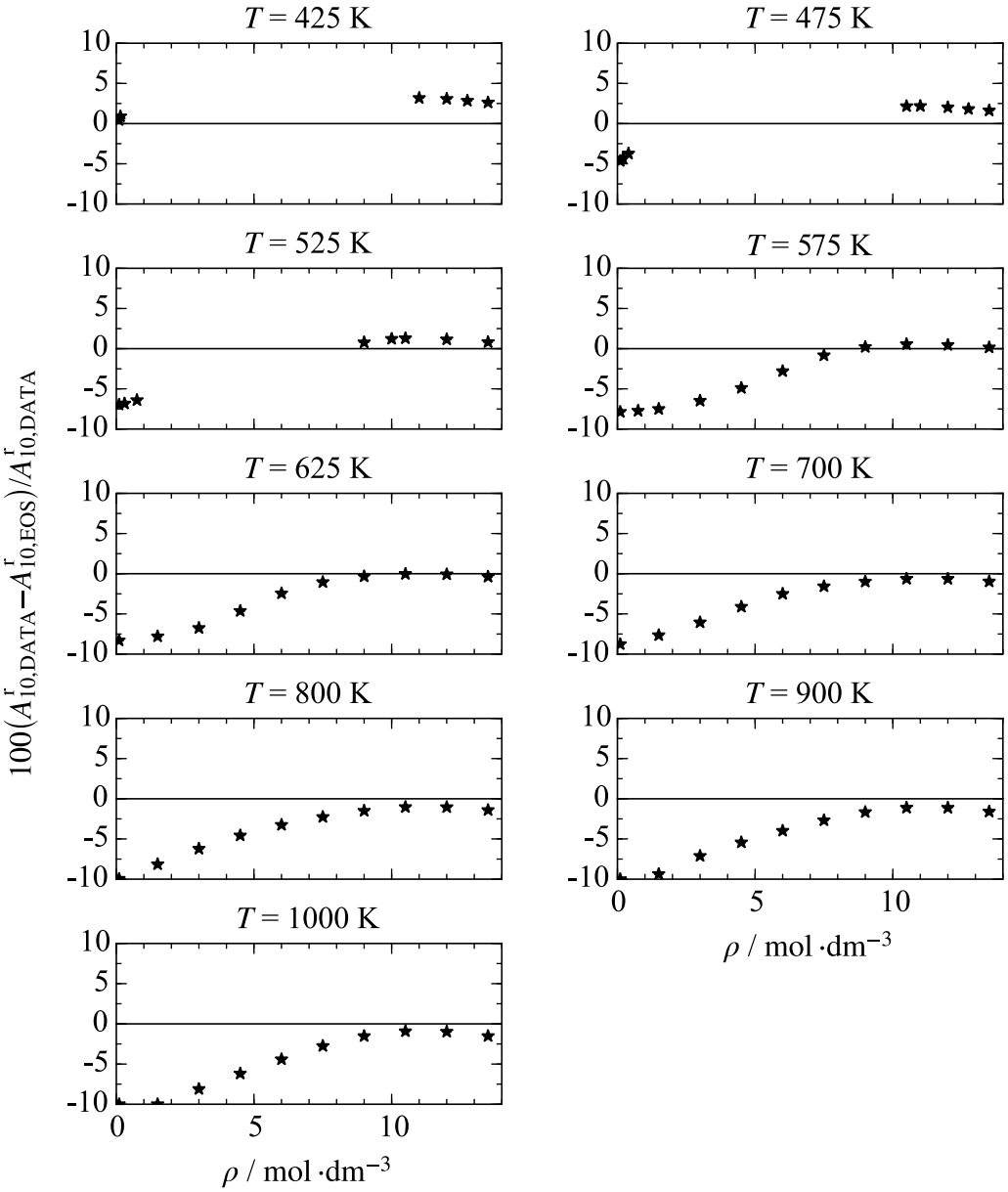


Figure S3. Relative deviation of simulated first derivative of the residual Helmholtz energy with respect to inverse temperature data from the present equation of state.

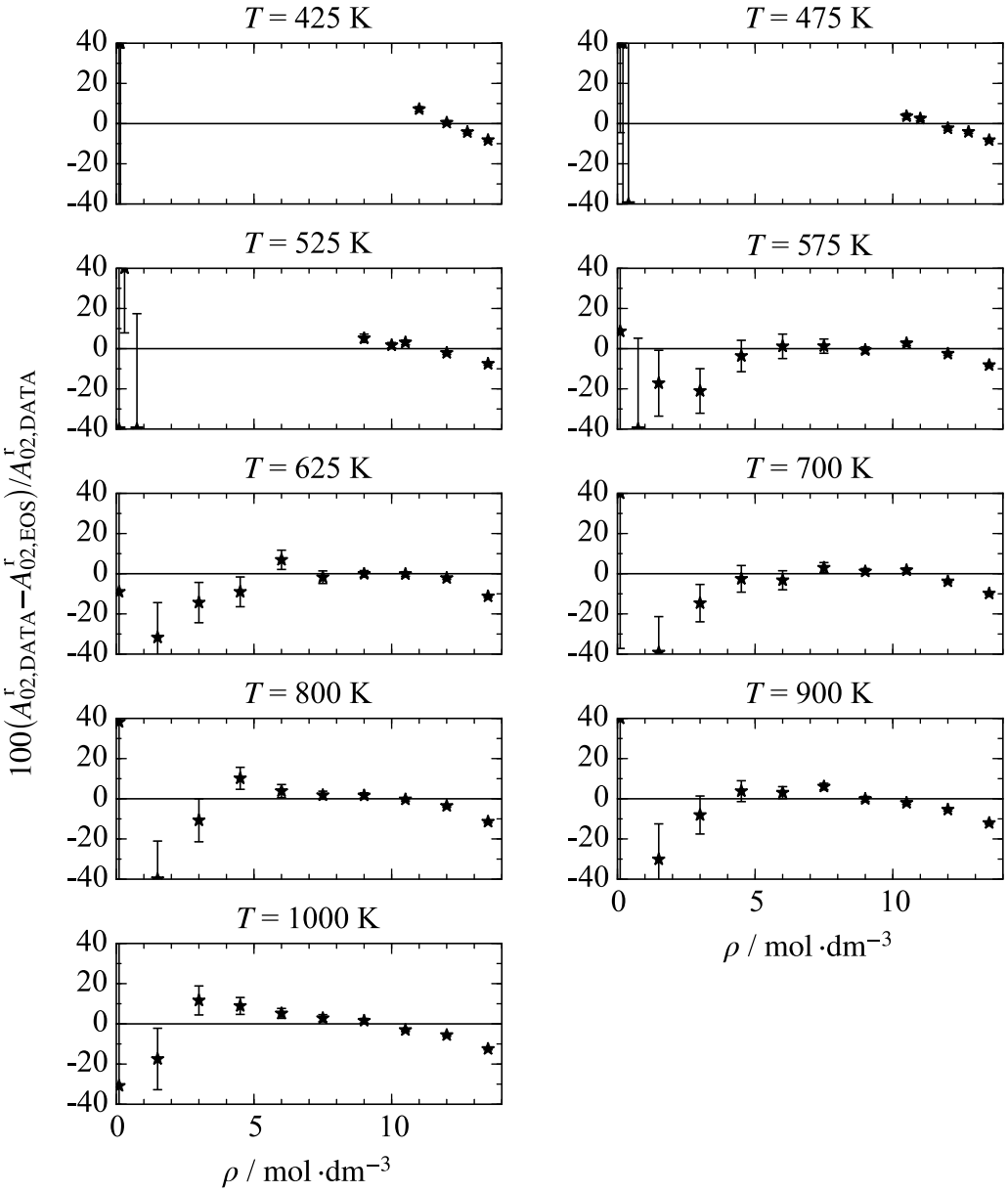


Figure S4. Relative deviation of simulated second derivative of the residual Helmholtz energy with respect to density data from the present equation of state.

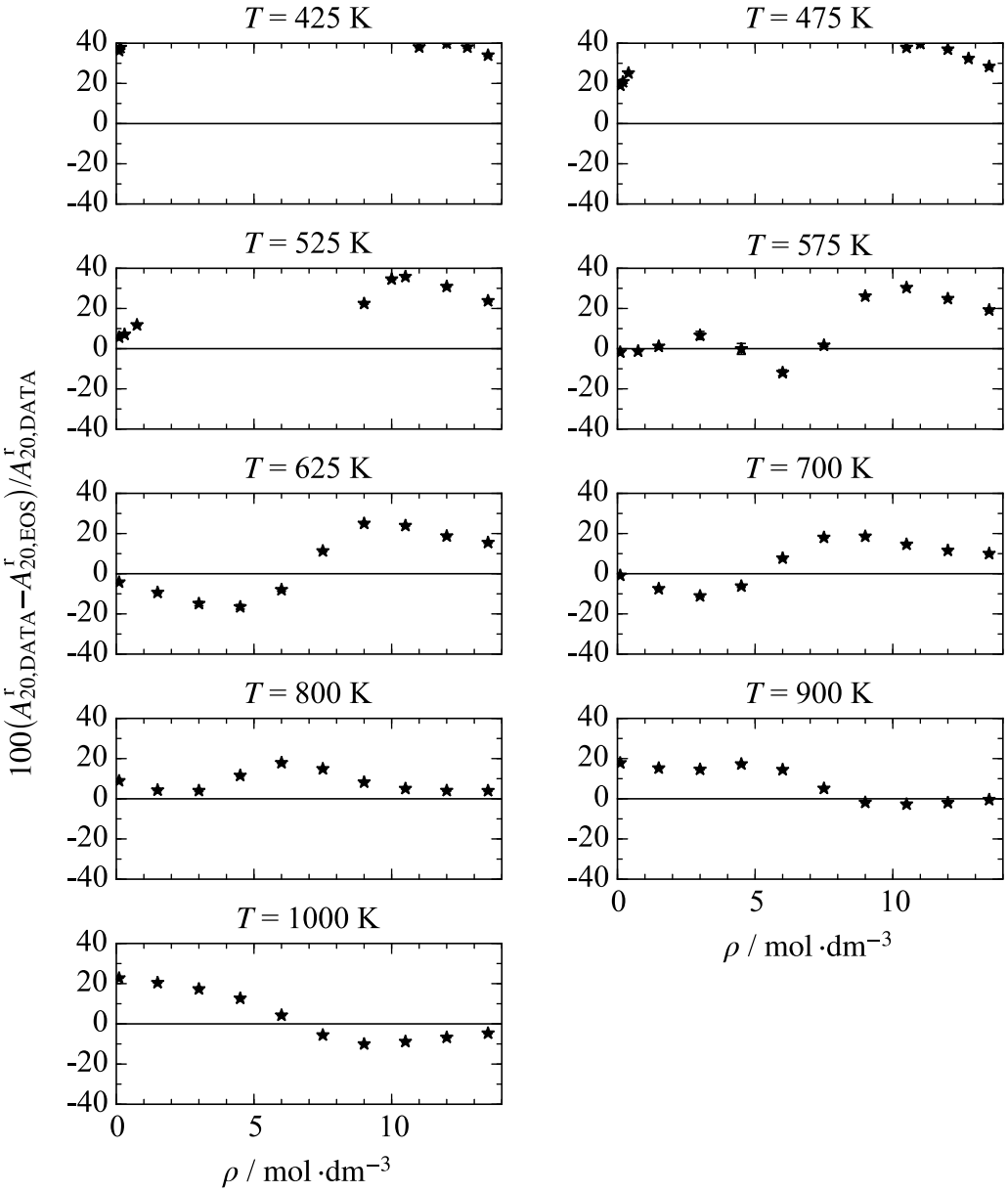


Figure S5. Relative deviation of simulated second derivative of the residual Helmholtz energy with respect to inverse temperature data from the present equation of state.

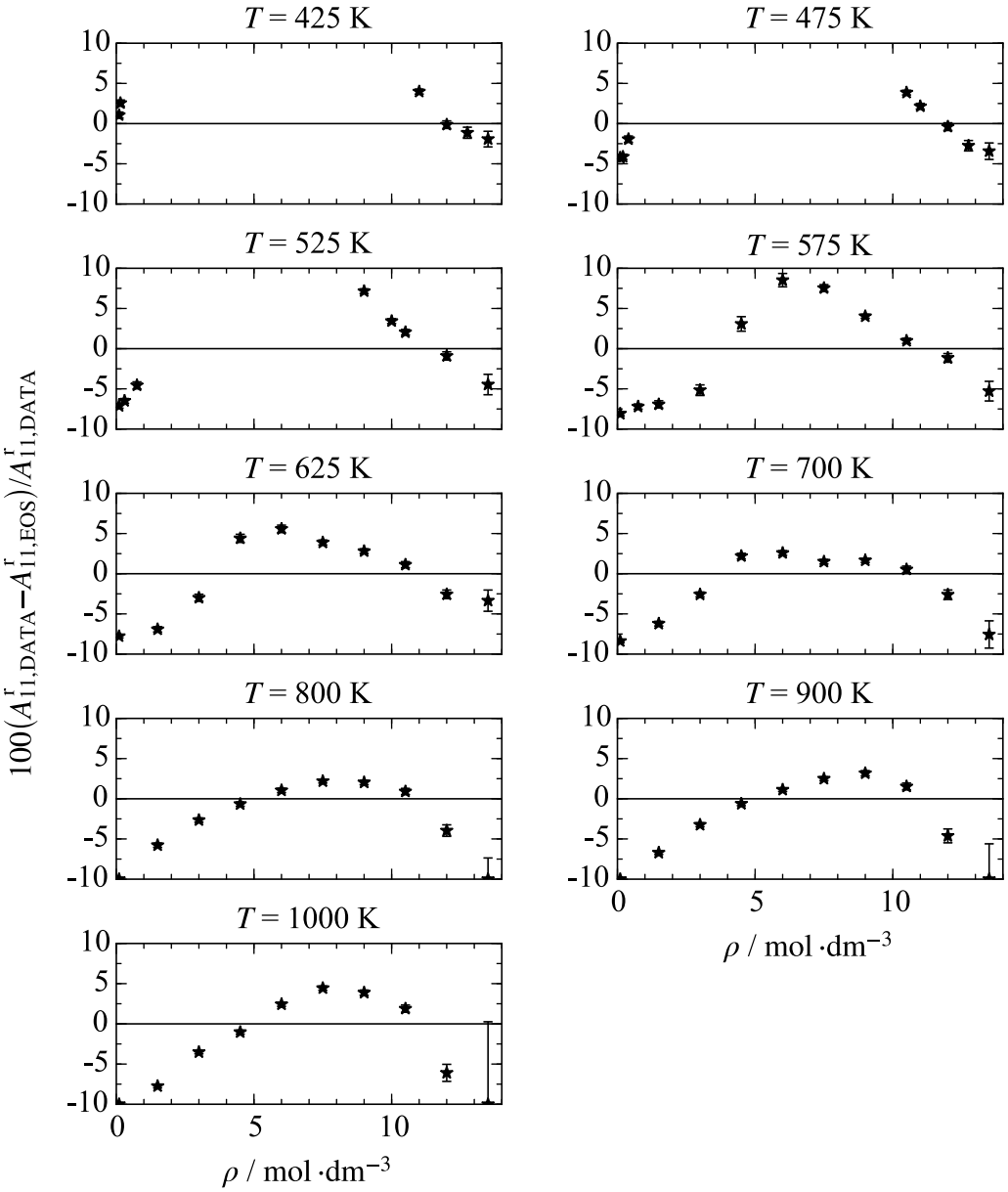


Figure S6. Relative deviation of simulated mixed derivative of the residual Helmholtz energy with respect to density and temperature data from the present equation of state.